

1 A new algorithm to accurately calculate neutral tracer gradients and their

2 impacts on vertical heat transport and water mass transformation

3 Sjoerd Groeskamp* and Paul M. Barker and Trevor J. McDougall

4 School of Mathematics and Statistics, University of New South Wales, Sydney, New South Wales,

5 Australia

6 Ryan P. Abernathey

7 Columbia University, Lamont-Doherty Earth Observatory, New York City, NY, USA

8 Stephen M. Griffies

9 NOAA Geophysical Fluid Dynamics Laboratory & Princeton University Program in Atmospheric

10 and Oceanic Sciences, Princeton, USA

11 *Corresponding author address: Sjoerd Groeskamp, School of Mathematics and Statistics UNSW

12 Sydney, NSW, 2052, Australia

13 E-mail: sjoerdgroeskamp@gmail.com

ABSTRACT

14 Mesoscale eddies stir along the neutral plane, and the resulting neutral diffu-
15 sion is a fundamental aspect of subgrid scale tracer transport in ocean models.
16 Calculating neutral diffusion traditionally involves calculating neutral slopes
17 and three-dimensional tracer gradients. The calculation of the neutral slope
18 usually occurs by computing the ratio of the horizontal to vertical locally ref-
19 erenced potential density derivative. This approach is problematic in regions
20 of weak vertical stratification, prompting the use of a variety of *ad hoc* reg-
21 ularization methods that can lead to rather nonphysical dependencies for the
22 resulting neutral tracer gradients. We here propose an alternative method that
23 is based on a search algorithm that requires no *ad hoc* regularization. Com-
24 paring results from this new method to the traditional method reveals large
25 differences in spurious diffusion, heat transport and water mass transforma-
26 tion rates that may all affect the physics of, for example, a numerical ocean
27 model. We end by concluding that the alternative method is more accurate,
28 both physically and numerically, thus suggesting it should form the basis for
29 future efforts involving neutral diffusion calculations from observations and
30 numerical model simulations.

31 **1. Introduction**

32 In the ocean, the neutral direction is the direction along which fluid elements can move a small
33 distance without experiencing a buoyant restoring force. The idea that ocean properties are ad-
34 vected and mixed predominantly along neutral directions has its origins in empirical observations
35 dating back at least to Iselin (1939), who was led to this insight from the similarities between ge-
36 graphically separated vertical casts in a salinity-temperature diagram. Recent presentations such
37 as in section 7.2 of Griffies (2004), section 2 of McDougall and Jackett (2005), and section 1 of
38 McDougall et al. (2014), argue that the very small dissipation of turbulent kinetic energy mea-
39 sured in the ocean interior by microstructure measurements supports the relevance of orienting
40 tracer mixing according to neutral and dianeutral directions. In particular, since it is generally
41 assumed that mesoscale turbulence produces little small-scale dissipation, mesoscale mixing is
42 constrained to occur in the neutral plane.

43 When mesoscale processes are not resolved, as in coarse-resolution ocean climate models, the
44 associated tracer mixing must be parameterized. The calculation of the neutral direction (neutral
45 slopes) forms a fundamental element of the subgrid scale parameterizations used in such mod-
46 els, as well as in observation-based watermass analyses. Neutral slopes arise in the formulation
47 of both the advective (or “skew”) component of parameterized mesoscale transport (Gent and
48 McWilliams 1990; Griffies 1998; McDougall and McIntosh 2001), as well as the neutral diffu-
49 sive component (Solomon 1971; Redi 1982; Griffies et al. 1998). Evidence from simulations has
50 shown that numerical ocean models are rather sensitive to details of both advective (Hirst et al.
51 1996; Gnanadesikan 1999; Marshall et al. 2017) and diffusive components (Pradal and Gnanade-
52 sikan 2014; Gnanadesikan et al. 2015). An accurate representation of the neutral direction is
53 therefore essential for an accurate implementation of the related ocean physics.

54 *a. The importance of neutral slopes*

55 As discussed by McDougall (1987a), neutral directions are the natural generalization of isopy-
 56 cnal surfaces, with the neutral direction tangent to the locally referenced potential density (ρ_l)
 57 surface. Due to a non-zero neutral helicity, which is an effect of the nonlinear equation of state,
 58 the neutral tangent plane (NTP) is always well-defined locally, while the extensive neutral surfaces
 59 have a nontrivial topology (McDougall and Jackett 1988). The resulting unit normal to the NTP, or
 60 dianeutral unit vector, is defined according to the gradient of locally referenced potential density
 61 ρ_l (McDougall et al. 2014)

$$62 \quad \mathbf{n} = -\frac{\nabla \rho_l}{|\nabla \rho_l|} = \frac{\alpha \nabla \Theta - \beta \nabla S_A}{|\alpha \nabla \Theta - \beta \nabla S_A|} = \frac{(\mathbf{S}, -1)}{\sqrt{S^2 + 1}}, \quad (1)$$

63 where the slopes of the NTP are given by

$$64 \quad \mathbf{S} = -\frac{\nabla_z \rho_l}{\partial_z \rho_l} = (S_x, S_y), \quad S^2 = \mathbf{S} \cdot \mathbf{S} = S_x^2 + S_y^2, \quad \nabla_z = \left(\frac{\partial}{\partial x}, \frac{\partial}{\partial y} \right). \quad (2)$$

65 Here S_A is the Absolute Salinity (McDougall and Jackett 2009), Θ the Conservative Temper-
 66 ature (McDougall 2003; Graham and McDougall 2013), and the locally referenced potential
 67 density $\rho_l = \rho(S_A, \Theta, P_r)$ is computed as in-situ density with respect to the local pressure P_r ;
 68 $\alpha = \alpha(S_A, \Theta, P)$ is the thermal expansion coefficient and $\beta = \beta(S_A, \Theta, P)$ is the haline contraction
 69 coefficient with units of K^{-1} and S_A^{-1} , respectively.

70 Traditional numerical methods use a finite-difference discretization of the normal direction \mathbf{n}
 71 of Eq. (2) as the basis for calculating neutral directions and related physical parameterizations
 72 (Marshall et al. 1997; Griffies et al. 1998; Shchepetkin and McWilliams 2005; Madec 2015). As
 73 we show in this paper, the traditional methods have nontrivial numerical issues related to this cal-
 74 culation. Due to the key role of eddy-induced neutral stirring and neutral diffusion for physical
 75 parameterizations, these numerical problems can have large impacts on the integrity of simula-
 76 tions, such as the vertical heat transport and water mass transformation.

⁷⁷ *b. Content of this paper*

⁷⁸ In this study, we present an alternative method for calculating neutral slopes and tracer gradi-
⁷⁹ ents. The new method is based on a search algorithm, rather than on the direct calculation of Eq.
⁸⁰ (2). We will compare and contrast the spurious diffusion induced by using either the traditional
⁸¹ vs. alternative methods, and compare the resulting estimates of heat transport and water mass
⁸² transformation. We find that the proposed alternative method is significantly more skilled, both
⁸³ physically and numerically, compared to the traditional methods.

⁸⁴ The structure of this paper is as follows. After we have detailed traditional methods for calcu-
⁸⁵ lating neutral slopes and neutral diffusion (Section 2a), we introduce our new method that is more
⁸⁶ accurate and does not require *ad hoc* choices that influence the results (Section 2b). The required
⁸⁷ discretization and algorithm that accompanies the alternative method are then discussed (Sections
⁸⁸ 3a and 3b). The different methods are then applied to a gridded ocean hydrography (Section 4a) in
⁸⁹ order to compare the resulting neutral tracer slopes and gradients (Section 4b and 4c), and for fic-
⁹⁰ titious diffusion (Section 4d), water mass transformation (Section 4e) and heat transport (section
⁹¹ 4f). After which we offer some concluding words (Section 5). Appendix 5 presents further details
⁹² of the algorithm.

⁹³ **2. Methods for calculating neutral diffusion**

⁹⁴ *a. The Traditional Method*

⁹⁵ Neutral diffusion is a fundamental part of the parameterization of subgrid scale mixing in models
⁹⁶ that do not resolve transient mesoscale eddies. A central component of neutral diffusion is a
⁹⁷ rotated diffusion operator that aligns tracer gradients according to neutral directions (Veronis 1975;
⁹⁸ Solomon 1971; Redi 1982; McDougall and Church 1986; Griffies et al. 1998; McDougall et al.

99 2014). The resulting downgradient tracer flux is given by

$$100 \quad \mathbf{F} = -K \nabla_{\mathbf{N}} C, \quad (3)$$

101 with K the neutral diffusivity (generally a tensor), C the tracer concentration, and $\nabla_{\mathbf{N}}$ the gradient
 102 operator aligned according to the neutral direction. In general we will use the notation $|_{\mathbf{N}}$ to
 103 indicate “along the neutral tangent plane (NTP)”. In practice, there are various methods used to
 104 compute $\nabla_{\mathbf{N}} C$, with nontrivial implications for the resulting diffusion operator.

105 We write the neutral tracer gradient in the form of an operator projecting out that portion of the
 106 three-dimensional tracer gradient aligned with the NTP (Olbers et al. 1986; Griffies et al. 1998;
 107 McDougall et al. 2014)

$$108 \quad \nabla_{\mathbf{N}} C = \nabla C - \mathbf{n} (\nabla C \cdot \mathbf{n}) = -\mathbf{n} \times (\mathbf{n} \times \nabla C). \quad (4)$$

109 Expanding equation (4) into a matrix-vector form leads to the following expression for the down-
 110 gradient neutral diffusion tracer flux

$$111 \quad -K \nabla_{\mathbf{N}} C = -K \frac{1}{1+S^2} \underbrace{\begin{pmatrix} 1+S_y^2 & -S_x S_y & S_x \\ -S_x S_y & 1+S_x^2 & S_y \\ S_x & S_y & S^2 \end{pmatrix}}_{\mathbf{N}} \begin{pmatrix} C_x \\ C_y \\ C_z \end{pmatrix} = -K \mathbf{N} \nabla C, \quad (5)$$

112 which reveals the role of the Redi diffusion tensor \mathbf{N} acting on the three-dimensional tracer gradient
 113 ∇C (Redi 1982). To reach this form we made the common assumption that the neutral diffusivity
 114 is isotropic in the neutral tangent plane (see Smith and Gent (2004) and Fox-Kemper et al. (2013)
 115 for discussions of anisotropic neutral diffusion). The three-dimensional convergence of this down-
 116 gradient diffusive flux then renders the neutral diffusion operator acting on the tracer C

$$117 \quad \mathcal{R}(C) = -\nabla \cdot (-K \nabla_{\mathbf{N}} C) = \nabla \cdot (K \mathbf{N} \nabla C). \quad (6)$$

¹¹⁸ For the numerical implementation of Eq. (6) it is common practice to use the small-slope approx-
¹¹⁹ imation to \mathbf{N} of Eq. (5) (Gent and McWilliams 1990). In the small-slope approximation, it is
¹²⁰ assumed that $(S_x S_y, S_x^2, S_y^2, S^2) \ll 1$, meaning that the angle between the neutral direction and the
¹²¹ horizontal is small, leaving¹

$$\mathbf{N}^{\text{small}} = \begin{pmatrix} 1 & 0 & S_x \\ 0 & 1 & S_y \\ S_x & S_y & S^2 \end{pmatrix}. \quad (7)$$

¹²³ The small-slope approximation is motivated both numerically and physically. Numerically,
¹²⁴ the small-slope approximation is less expensive to calculate. Physically it is motivated since
¹²⁵ mesoscale eddies generally mix horizontally rather than neutrally when encountering regions of
¹²⁶ near vertical neutral directions, such as in the mixed layer, in which case neutral diffusion reverts
¹²⁷ to horizontal diffusion (Treguier et al. 1997; Ferrari et al. 2008; Danabasoglu et al. 2008; Ferrari
¹²⁸ et al. 2010).

¹²⁹ McDougall et al. (2014) showed that the small-slope approximation to the full tensor is not
¹³⁰ exactly in the direction of the correct neutral tracer gradient, but the related error is tiny and of
¹³¹ negligible physical consequence. Therefore, to a good approximation, the neutral tracer gradient
¹³² is given by:

$$\nabla_{\mathbf{N}} C \approx \mathbf{N}^{\text{small}} \nabla C = \nabla_{\mathbf{n}} C + \hat{\mathbf{z}} (\nabla_{\mathbf{n}} C \cdot \nabla_n z) = \nabla_{\mathbf{N}}^{\text{small}} C. \quad (8)$$

¹³⁴ where

$$\nabla_{\mathbf{n}} C = \nabla C - \mathbf{m} \frac{\partial C}{\partial z}, \quad \text{with} \quad \mathbf{m} = -\nabla_n z + \hat{\mathbf{z}} \quad \text{and} \quad \nabla_n z = (S_x, S_y). \quad (9)$$

¹It is important to retain the (3,3) component in equation (7) as it combines with the vertical diffusivity arising from dianeutral processes.

¹³⁶ The three-dimensional convergence of this downgradient small-slope diffusive flux then renders
¹³⁷ the neutral diffusion operator acting on the tracer C

¹³⁸
$$\mathcal{R}^{\text{small}}(C) = -\nabla \cdot \left(-K \nabla_{\mathbf{N}}^{\text{small}} C \right) = \nabla \cdot \left(K \mathbf{N}^{\text{small}} \nabla C \right). \quad (10)$$

¹³⁹ In Eq. (8) we used is the two dimensional projected nonorthogonal neutral tracer gradient $\nabla_{\mathbf{n}} C$,
¹⁴⁰ which was first introduced by Starr (1945) and has since been widely used in geophysical fluid the-
¹⁴¹ ory and modeling. Isopycnal ocean models (Bleck 1978a,b) compute isopycnal tracer diffusion by
¹⁴² taking the two-dimensional convergence of $-K \nabla_{\mathbf{n}} C$ along isopycnal layers. This approach con-
¹⁴³ trasts to that of geopotential coordinate models, which compute the 3D-convergence of $-K \nabla_{\mathbf{N}}^{\text{small}} C$
¹⁴⁴ as in Eq (10). However, the two approaches can be shown to be mathematically identical under the
¹⁴⁵ small-slope approximation, and so the different approaches arise from convenience rather than fun-
¹⁴⁶ damentals. Whether one uses $\nabla_{\mathbf{n}} C$ or $\nabla_{\mathbf{N}} C$, the integrity of a numerical neutral diffusion scheme
¹⁴⁷ relies on an accurate representation of the neutral slope.

¹⁴⁸ Fundamental to the Redi tensor is the computation of the slope of the NTP relative to the hori-
¹⁴⁹ zontal plane (S_x and S_y). The slope of the NTP, or “neutral slope”, is traditionally written as the
¹⁵⁰ ratio of horizontal to vertical derivatives of the locally referenced potential density (Eq. 2). In
¹⁵¹ practice the calculation of the neutral slope according to equation (2) can be problematic, with
¹⁵² problems arising from division by $\partial \rho_l / \partial z$ in regions where the vertical stratification is weak (Fig.
¹⁵³ 1). This division results in an unbounded neutral slope that thus requires some form of numerical
¹⁵⁴ regularization such as those proposed by Cox (1987), Gerdes et al. (1991), and Danabasoglu and
¹⁵⁵ McWilliams (1995). Depending on the regularization chosen, one can realize an overly small or
¹⁵⁶ overly large neutral tracer gradient. Numerical simulations are sensitive to the (arbitrary) choice
¹⁵⁷ for the slope regularization (e.g., Griffies et al. 2005; Gnanadesikan et al. 2007; Ferrari et al. 2008),
¹⁵⁸ thus leading to a rather unfortunate sensitivity to a generally *ad hoc* numerical scheme. In addi-

159 tion, slope regularizations such as that proposed by Cox (1987) can lead to spurious dianeutral
 160 transports (though the methods of Gerdes et al. (1991) and Danabasoglu and McWilliams (1995)
 161 avoid this problem).

162 *b. Our Alternative Method*

163 We consider the use of *ad hoc* slope regularizations to be unsatisfying both physically and nu-
 164 mercially. We thus seek an alternative approach to calculate neutral slopes and related neutral
 165 tracer gradients. For this purpose, rather than starting from Eq. (2) for the neutral slope, we start
 166 from the mathematically identical form

$$167 \quad S_x = \left(\frac{\partial z}{\partial x} \right)_{y,N} \quad S_y = \left(\frac{\partial z}{\partial y} \right)_{x,N}. \quad (11)$$

168 This expression for the slope is based on directly computing the change in depth of a neutral
 169 direction when moving laterally along a NTP, hence $|_{y,N}$ indicates "along the NTP, at constant y".
 170 Correspondingly, neutral tracer gradients can also be obtained by directly computing the change
 171 in tracer values when moving (laterally) along a NTP, leaving

$$172 \quad \nabla_N^{\text{small}} C = \left(\frac{\partial C}{\partial x} \Big|_{y,N}, \frac{\partial C}{\partial y} \Big|_{x,N}, \frac{\partial C}{\partial z} \Big|_N \right). \quad (12)$$

173 To calculate the neutral direction and neutral tracer gradients according to Eqs. (11) and (12)
 174 respectively, we make use of a search algorithm. For a finite resolution dataset from, for example,
 175 a numerical model or an observational analysis, the goal of the algorithm is to find the intersection
 176 of a NTP between adjacent fluid columns (Fig. 1, details are given in section 3b). Knowing the
 177 intersection of one NTP on two adjacent fluid columns allows us to estimate the height and tracer
 178 values at these locations, which can subsequently be used to calculate both the neutral slopes and
 179 neutral tracer gradients. Notably, the search generally spans multiple vertical grid cells, which
 180 contrasts to the vertically local methods based on the slope calculation starting from equation (2).

181 Very steep NTPs may intersect the surface or bottom before reaching the adjacent column, and
182 thus are effectively vertical.

183 In the following sections, we will compare the three following methods to calculate neutral
184 tracer gradients:

185 1. **The local-method:** This is the method that has been referred to as the traditional method
186 (section 2a), but will hereafter be referred to as “the local-method”. For the local-method,
187 Eq. (8) is used to calculate the neutral gradients. Both the calculation of the slopes (according
188 to Eq. (2)) and tracer gradients are based on the local grid stencil discretization of the vertical
189 and horizontal derivatives. The neutral slopes and tracer gradient of the local-method are
190 represented as $\nabla_N^{\text{local}} C = \mathbf{N}_{\text{local}}^{\text{small}} \nabla_{\text{local}} C$

191 2. **The non-local method:** The non-local method is an algorithm that finds the intersections of
192 a NTP between two vertical casts. The difference between tracer values and height at both
193 intersections provides a direct estimate of the neutral tracer gradient and slope according to
194 Eqs. (11) and (12). The details of this algorithm are described in Section 3b. This method
195 can reach vertically to distant grid cells for estimating the NTP, thus earning the non-local
196 moniker. The neutral slopes and tracer gradient of the non-local method are represented as
197 $\nabla_N^{\text{nloc}} C$ and \mathbf{S}^{nloc} , respectively. Although \mathbf{S}^{nloc} is not needed to calculate neutral gradients,
198 it can however be used for other purposes such as for parameterized eddy-induced stirring
199 (Gent et al. 1995).

200 3. **The hybrid-method:** The hybrid-method employs Eq. (8), the small slope approximation, to
201 calculate the neutral gradients but employs the more accurate neutral slopes resulting from the
202 non-local method (rather than the local version from Eq. (2)). The neutral slopes and tracer
203 gradient of the hybrid method are represented as $\nabla_N^{\text{hybrid}} C = \mathbf{N}_{\text{nloc}}^{\text{small}} \nabla_{\text{local}} C$, where $\mathbf{N}_{\text{nloc}}^{\text{small}}$

uses \mathbf{S}^{nloc} . The hybrid-method serves to illustrate whether the local-method suffers only from numerical issues arising from calculating slopes according to Eq. (2), or also suffers from the fact that local extrema in Cartesian tracer gradients can lead to numerical errors. Note that due to the independent means by which the slopes and Cartesian tracer gradients are obtained, the hybrid-method is not self-consistent. That is, there may be small amounts of unphysical diffusion as a result of this inconsistency as detailed in Griffies et al. (1998).

210 c. Slope Regularization

211 Coarse resolution prognostic ocean models commonly make use of neutral diffusion schemes
212 with neutral slopes based on equation (2), i.e. the local-method. For these models, one generally
213 sets the maximum neutral slope according to numerical time stepping stability constraints rather
214 than on numerical accuracy considerations (see discussions in Cox 1987; Griffies 1998; Lemarié
215 et al. 2012). However, numerical stability does not imply numerical accuracy. Indeed, the calcula-
216 tion of neutral slopes using the local-approach is inaccurate for slopes steeper than the grid aspect
217 ratio $\Delta z / \Delta x$. The reason is that the method makes use only of information that is vertically local,
218 and so neutral slopes steeper than the grid aspect ratio extend beyond a single adjacent cell in the
219 vertical. A local calculation of neutral slopes steeper than the grid aspect ratio makes use of an
220 extrapolation, which is fundamentally less accurate than interpolation.

221 The non-local method proposed in this study always interpolates as part of estimating neutral
222 slopes (except for cases when NTP outcrops into the atmosphere or incrops into the bottom, Ap-
223 pendix 5). In so doing, slope regularization is intrinsic to the non-local method as the maximum
224 slope is limited by the ratio of the depth of the ocean (H) to the horizontal resolution of the data
225 set. In effect, it replaces the *ad hoc* slope regularization required by the local-method with a reg-
226 ularization based on using only that information directly available from the discrete grid, without

227 extrapolation. By searching over an arbitrary number of vertical grid cells in adjacent columns, the
228 non-local method can estimate steep neutral slopes more accurately than the local-method, which
229 is vertically local (Fig. 1). That is, where there could be a significant neutral tracer gradient over
230 the grid scale, there may locally be a weak gradient.

231 Without some form of quantification of the effects of the different methods on ocean physics,
232 it is not obvious that one approach is fundamentally better than the other. As explained above,
233 the local-method calculates the neutral direction locally (as defined by Eq. (2), but suffers from
234 numerical issues (extrapolation, regularization) due to the finite resolution of a discrete data set.
235 The non-local method can be considered "less fundamental" through its vertical non-locality in the
236 calculation of the neutral directions. However, as we will show, it suffers far less from numerical
237 inaccuracies and arbitrariness, with the result being far more physically sensible results.

238 As shown in this paper, these algorithm details have important implications for the calculation
239 of diagnostic analyses of observation-based data. By extension, we conjecture that the same issues
240 and sensitivities arise for parameterized tracer transport in prognostic ocean models.

241 3. Implementation of the Non-Local Method

242 a. The Finite Difference Expressions

243 The new algorithm (Section 3b) calculates neutral slopes (\mathbf{S}) and neutral gradients of S_A , Θ and
244 pressure P . The algorithm is specifically designed for a z-grid coordinate discretization of a tracer
245 C . The algorithm provides neutral gradients and slopes on predetermined locations between two
246 vertical casts. The neutral slopes are calculated using the finite-difference approximation of Eq.
247 (11):

$$\left. S_x^{\text{nloc}} = \frac{\Delta z}{\Delta x} \right|_{y, N} \quad \left. S_y^{\text{nloc}} = \frac{\Delta z}{\Delta y} \right|_{x, N} . \quad (13)$$

249 Here $|_{y,N}$ ensures that Δz is the change in height of the NTP over the horizontal distance Δx . The
 250 search algorithm determines the vertical distance Δz , whereas the spatial resolution provides the
 251 horizontal distances Δx and Δy . As a result, the maximum slopes that can be obtained are when
 252 $\Delta z = H$ equals the depth of the ocean; i.e., a NTP that extends from the bottom of one column to
 253 the top of an adjacent column. Smaller effective S_{\max} arises for points that are within the ocean
 254 interior. For a 1° degree spatial resolution and a 5000 m deep ocean, this provides $S_{\max} \approx 0.05$ as
 255 an example for the natural neutral slope regularization embedded in the non-local method.

256 In the algorithm we make use of the small-slope approximation of the neutral gradients of Eq.
 257 (8):

$$258 \quad \nabla_N^{\text{small}} C \cdot \hat{\mathbf{x}} = \frac{\partial C}{\partial x} \Big|_{y,N} = \frac{\partial C}{\partial x} + S_x \frac{\partial C}{\partial z} \quad (14)$$

$$259 \quad \nabla_N^{\text{small}} C \cdot \hat{\mathbf{y}} = \frac{\partial C}{\partial y} \Big|_{x,N} = \frac{\partial C}{\partial y} + S_y \frac{\partial C}{\partial z} \quad (15)$$

$$260 \quad \nabla_N^{\text{small}} C \cdot \hat{\mathbf{z}} = \frac{\partial C}{\partial z} \Big|_N = S_x \frac{\partial C}{\partial x} + S_y \frac{\partial C}{\partial y} + S^2 \frac{\partial C}{\partial z}. \quad (16)$$

261 Here $\hat{\mathbf{x}}$, $\hat{\mathbf{y}}$ and $\hat{\mathbf{z}}$ are the unit normal vectors in the x , y and z directions, respectively. Discretizing
 262 Eq. (14) renders:

$$263 \quad \frac{\partial C}{\partial x} + S_x \frac{\partial C}{\partial z} = \frac{\Delta C|_{y,z}}{\Delta x} + \frac{\Delta z}{\Delta x} \Big|_{y,N} \frac{\Delta C|_{x,y}}{\Delta z} = \frac{1}{\Delta x} \left[\frac{\Delta C|_{y,z}}{\Delta x} \Delta x + \frac{\Delta C|_{x,y}}{\Delta z} \Delta z \right] = \frac{\Delta C|_{N,y}}{\Delta x}. \quad (17)$$

264 Again, $\Delta C|_{y,z}$ indicates the temperature difference in the x -direction at constant y and z . Hence,
 265 $\frac{\Delta C|_{N,y}}{\Delta x}$ is the gradient of C along the NTP in the x -direction. Using Eqs. (14) - (16) we rewrite $\nabla_N C$
 266 as:

$$267 \quad \nabla_N^{\text{nloc}} C = \left(\frac{\Delta C|_{N,y}}{\Delta x}, \frac{\Delta C|_{N,x}}{\Delta y}, S_x^{\text{nloc}} \frac{\Delta C|_{N,y}}{\Delta x} + S_y^{\text{nloc}} \frac{\Delta C|_{N,x}}{\Delta y} \right). \quad (18)$$

268 In Section 3b we discuss how the algorithm provides S_x^{nloc} , S_y^{nloc} , $\Delta C|_{N,y}$ and $\Delta C|_{N,x}$.

269 *b. The Search Algorithm*

270 Here we present the algorithm to calculate neutral slopes (S_x^{nloc} and S_y^{nloc}) and neutral gradients
 271 ($\Delta C|_{N,y}$ and $\Delta C|_{N,x}$), where C will later be replaced by S_A , Θ or P . This section is mostly con-
 272 ceptual, with the technical details provided in Appendix 5. We start by considering a north-south
 273 transect, at constant longitude, with sufficient vertical resolution (Fig. 1), and

274
$$\Delta y = y_{\text{north}} - y_{\text{south}} \quad \Delta z = z_{\text{north}} - z_{\text{south}} \quad \Delta C|_{N,x} = (C_{\text{north}} - C_{\text{south}})_N. \quad (19)$$

275 We will construct a finite length NTP between these two neighboring vertical casts, such that C_{south}
 276 and C_{south} represent the values of tracer C at the intersection of the NTP with the south and north
 277 cast, respectively. A NTP is defined with respect to a local reference pressure P_r . We choose
 278 to define the NTP with respect to the mid-pressure $P_m = 0.5(P_{\text{south}} + P_{\text{north}})$, at the mid-latitude
 279 $y_m = 0.5(y_{\text{south}} + y_{\text{north}})$ between the casts. Consequently, the related neutral gradients are also
 280 defined at the (P_m, y_m) . We apply two main steps, 1) - iteration to find a neutral surface, and 2)
 281 iteration to find the neutral surface that crosses through the pre-determined grid-point.

282 1) STEP 1: FINDING A NEUTRAL TANGENT PLANE

283 In the first step of the algorithm we find the finite difference NTP. To do so, the intersection
 284 of the NTP with the south cast is fixed at a T-grid, i.e., the locations where tracers are given
 285 (Fig 10 of Appendix 5). We provide an initial guess of the height of the intersection of the NTP
 286 with the north-cast. From both south and north intersections, we apply an adiabatic and isohaline
 287 displacement of fluid parcels (i.e. Θ and S_A are constant, but P is not) to their mid-pressure P_m at
 288 y_m . The difference in the specific volume of seawater ($v = \rho^{-1}$) between the two displaced fluid
 289 parcels, with respect to their mid-pressure, is then given by

290
$$\Delta v = v(S_{A,\text{north}}, \Theta_{\text{north}}, P_m) - v(S_{A,\text{south}}, \Theta_{\text{south}}, P_m) \quad (20)$$

291 Here Δv measures whether the parcels are on the same NTP with respect to P_m . A larger value
 292 of $|\Delta v|$ indicates that both parcels are not on the same NTP (different ρ_l). Hence, by finding an
 293 intersection for which $\Delta v = 0$, we can consider both intersections to be on the same ρ_l -surface,
 294 i.e., they are on the same NTP.

295 Note, we deliberately chose to use v instead of ρ . This choice is motivated by two reasons; 1)
 296 arguably, it is more appropriate to define a quantity relative to a conserved variable rather than to
 297 a non-conserved variable. Because mass is a conserved rather than volume, the more appropriate
 298 variable to consider is v rather than ρ ,² and 2) the McDougall and Barker (2011) software calcu-
 299 lates $v(S_A, \Theta, P)$ using a simple polynomial, making it is more computational efficient to find the
 300 partial derivatives of v than it is to find the corresponding partial derivatives of ρ .

301 The algorithm finds an approximate NTP over a finite distance Δy , between two vertical casts.
 302 As a NTP is only locally defined (Eq. 2), it is unexpected to find cases for which $\Delta v = 0$. For
 303 any practical purposes, the NTP can therefore only be determined within a certain predefined
 304 accuracy. We achieve this accuracy by using an algorithm that searches iteratively, while using
 305 linear interpolation between vertical grid points, for a location on the north cast (with the south-
 306 cast intersection fixed) that satisfies

$$307 \quad \Delta v \leq \underbrace{v_{\text{crit}} = 10^{-12} \text{ m}^3 \text{ kg}^{-1}}_{\text{criteria}}. \quad (21)$$

308 The accuracy that we employ is $v_{\text{crit}} = 10^{-12} \text{ m}^3 \text{ kg}^{-1}$. For a hydrostatic fluid, the buoyancy
 309 frequency is given by $N^2 \approx \frac{g^2 \Delta \rho}{\Delta P}$. Combining with $\Delta \rho \approx \rho^2 \Delta v$ and $\Delta v = v_{\text{crit}}$ leads to $\Delta P \approx$
 310 $g^2 \rho^2 v_{\text{crit}} / N^2 \approx 0.1 \text{ dbar}$ for $N^2 = 1 \times 10^{-7} \text{ s}^{-2}$. This result can be interpreted as a mismatch
 311 between the two neutral tangent planes at the mid-point pressure P_m of at most 10 cm in regions

²Considering the non-conservation of ρ is considering the non-conservation of the reciprocal of volume, which is not conserved. Graham and McDougall (2013) showed that for the full range of oceanic S_A , Θ and P combinations, turbulent mixing always destroys v , but does not always produce ρ .

312 of weak stratification. The current choice of accuracy is one that balances computational cost and
313 accuracy (more accurate, requires more computation). Once a NTP is constructed, we can use
314 the values of the depth z of both end points to calculate the slope, while we use the values of the
315 tracers (Θ, S_A, P) to calculate the gradients. In the next step we will discuss how to obtain these
316 results *on* the mid-point of the interface.

317 2) STEP 2: FINDING THE NEUTRAL TANGENT PLANE AT A TARGET PRESSURE.

318 In the previous step, we have found an approximate NTP connecting a T-grid point on the south-
319 cast to a particular location on the north-cast. In other words, P_{south} was fixed, while the location
320 of the north-cast varied. As a result, P_m , where the neutral slopes and gradients are defined at, is
321 most likely not on the same pressure as the T-grid itself.

322 For the calculations of budgets, and tracer transports into and out of the T-grid volumes, the
323 neutral slopes and gradients are required to be defined at the middle of the interfaces surrounding
324 the T-grid (Griffies 2012; Madec 2015). For the vertical interfaces this is at the same pressure as
325 the T-grid, but at a different longitude or latitude. For the horizontal interfaces this is at the same
326 longitude and latitude, but at the average pressure between two vertically spaced T-grid points (Fig
327 10 of Appendix 5). The goal of step 2 is to obtain neutral slopes and gradients that are defined at
328 the specified pressure.

329 We will proceed with the example of obtaining neutral slopes and gradients in the y-direction.
330 We identified two options on how to proceed. For the first option we construct NTP's for each T-
331 grid point (numbers will depend on the vertical resolution), and calculate the related neutral slopes
332 and gradients on the interfaces. The neutral slopes and gradients are then interpolated exactly onto
333 the pre-determined pressures that correspond to the same pressure as the T-grid. For the second
334 option, we use an iterative process in which we also move the starting location vertically along the

335 south-cast, in order to search for a NTP that crosses through the pre-determined pressures on the
336 interface.

337 Because NTPs are defined locally, we adopt the second option as this provides a more local and
338 therefore arguably more accurate solution. We adopt a minimum accuracy of 50 cm, meaning that
339 NTPs have to cross the pre-determined pressures within 50 cm distance. The numerical details of
340 this iterative process are provided in Appendix 5. After the algorithm has found the intersection
341 of the NTP with the two casts, for the given criteria, the z , S_A , Θ and P at the intersections is
342 determined to provide S_y^{nloc} and $\Delta C|_{N,x}/\Delta y$. The exact same method is applied for the x -direction
343 to obtain S_x^{nloc} and $\Delta C|_{N,y}/\Delta x$. From the combination of the tracer gradients and slopes in the x
344 and y direction and some horizontal averaging, we can calculate the vertical components of Eq.
345 (18) on the horizontal surfaces.

346 4. Comparison of the Different Methods

347 a. Data

348 The observationally based climatology is given by monthly means of the World Ocean Atlas
349 2013, which is a set of objectively analyzed (1° grid) climatological fields of *in-situ* temperature,
350 Practical Salinity, and other tracers at standard depth levels for the world ocean (Boyer et al. 2013).
351 TEOS-10 software (IOC et al. 2010; McDougall and Barker 2011) is applied to convert the data to
352 S_A and Θ , achieve static stability (Barker and McDougall 2017), and obtain Neutral Density (not
353 available north of 64°N , Jackett and McDougall 1997). For this dataset we have calculated slopes
354 and gradients using the three methods described above. In addition to the methods mentioned
355 before, we have also applied a similar algorithm as the direct method to find surfaces of potential
356 density anomaly referenced to 2000 dbar, i.e. $\sigma_2 = \rho(S_A, \Theta, P = 2000) - 1000 \text{ kg m}^{-3}$. This cal-

357 culation allows us to estimate the effects of non-neutrality when choosing σ_2 as an approximation
358 to a neutral surface. We have excluded the Arctic region from this analysis, as the present data in
359 that area does not allow for the calculation of physically realistic gradients with any method.

360 *b. Comparing the neutral slopes.*

361 The most fundamental variables to compare between the local-method and the non-local method
362 are the neutral slopes in the x and y directions. We emphasize that the neutral slopes calculated
363 using the local method are capped with a maximum value of $|\max(S_x, S_y)| = 0.01$ and about 2.8%
364 and 1.8% of the data exceeded the slope limit in the x and y , respectively. In calculating σ_2 the
365 slopes in the x -direction were capped to 0.02. The number 0.02 was based on the maximum slopes
366 found in the y -direction, which were not capped. For the non-local method and hybrid-method, no
367 regularization is applied to either the slopes or the gradients.

368 A map and transect of the neutral slopes in January (Figs. 2), show that the slopes resulting from
369 the local-method, non-local method and σ_2 , all show very similar spatial patterns. The slopes vary
370 in magnitude more irregularly and on smaller spatial scales in the x direction than in the y direction.
371 However, it is clear that the slopes in especially the local-method are more “spikey” compared to
372 the much smoother patterns of the non-local method and that from σ_2 . Clear examples of such
373 behavior can be found by comparing the slopes in the Southern Ocean both horizontally and at
374 different depths (South of 40°S, Fig. 2).

375 We note that the maximum values found by using the local method are slopes up to 200, which
376 are practically vertical. The slopes that are capped to the slope limit are the largest slopes found
377 in the ocean. Given that these steep slope regions often correspond to strong vertical transport,
378 they are quite important for the calculation of tracer gradients using Eq. (5). Hence, not only is

379 the local-method less accurate, but any physics calculated using $\nabla_N^{\text{local}} C$ will be sensitive to the *ad*
380 *hoc* choice of the maximum slope.

381 *c. Comparing the neutral gradients.*

382 There are now four different estimates of the neutral tracer gradients (non-local method, hybrid-
383 method, local-method and from σ_2). We discuss the neutral Θ gradients ($\nabla_N \Theta$) in x , y and z
384 direction, for the different methods (Figs. 3, 4 and 5). We note that (not shown), the gradients
385 for S_A have very similar patterns and characteristics, while the gradients for P are very similar to
386 the slopes, but with the opposite sign. The general patterns for the gradients for all methods are
387 very similar. Gradients in the x -direction (Fig. 3) are more irregular than those in the y -direction
388 (Fig. 4). The component of the neutral gradients in both x and y gradients are about 3 orders of
389 magnitude larger than the component of the gradients in the z -direction (Fig. 5).

390 It is important to consider the structure of the Θ -gradients in x and y direction, south of 50°S
391 (transect), between the surface and about 600 m depth. These are some of the largest neutral
392 gradients found in the ocean, due to the steep neutral slopes and strong temperature changes across
393 the fronts of the Antarctic Circumpolar Current (Figs. 3 and 4). Here the non-local method leads to
394 smoother and arguably more realistic and accurate gradients than any of the other methods. As the
395 neutral Θ gradient in the z -direction is a linear combination of the gradients in the x and y -direction,
396 inaccuracy in the x and y directions translate to inaccuracies of gradients in the z direction. These
397 inaccuracies turn out to be especially troublesome for the vertical eddy heat-fluxes.

398 *d. Fictitious Diffusion*

399 By definition, for an *exact* NTP we have

$$L = -\alpha \nabla_N \Theta + \beta \nabla_N S_A = 0. \quad (22)$$

400 Here \mathbf{L} has units of inverse length and $\rho\mathbf{L}$ can be interpreted as the change in locally referenced
 401 potential density, per meter, due to non-neutrality. Even the best discrete approximation of the
 402 NTPs is not exact, so that the approximate value for $\mathbf{L} \neq 0$. Following Klocker et al. (2009),
 403 we turn this nonzero \mathbf{L} into an expression for fictitious diffusivity D_f . Doing so provides an
 404 independent measure and interpretable variable that can assess the neutrality of the neutral gradients
 405 as obtained by the different methods.

406 The fictitious diffusivity is given by (Klocker et al. 2009)

$$D_f = K \cdot (\nabla_N z - \nabla_a z)^2. \quad (23)$$

407 Here K is a mesoscale eddy diffusivity that parameterizes stirring by mesoscale eddies along the
 408 NTP, for which we choose the canonical value of $K = 1000 \text{ m}^2 \text{ s}^{-1}$ (even though it may vary spa-
 409 tially, Abernathey and Marshall 2013; Klocker and Abernathey 2013; Cole et al. 2015; Groeskamp
 410 et al. 2017; Roach et al. 2018). The term $\nabla_N z - \nabla_a z$ represents the difference between the slope of
 411 the exact NTP ($\nabla_N z$) and the approximate NTP ($\nabla_a z$). When the approximate NTP is not exactly
 412 neutral, then diffusion along the approximate NTP leads to a dianeutral transport through the ex-
 413 act NTP, that can be expressed using fictitious diffusivity D_f . To calculate D_f , the slope difference
 414 $\nabla_N z - \nabla_a z$ is first approximated as the height difference along a NTP (Δz_N) minus the height dif-
 415 ference of the approximate NTP (Δz_a). Using a finite horizontal distance $d_h = \sqrt{(\Delta x)^2 + (\Delta y)^2}$,
 416 this height difference between the NTP and the approximate NTP is given by

$$\nabla_N z - \nabla_a z \approx \frac{\Delta z_N - \Delta z_a}{d_h} = \frac{\Delta z_\epsilon}{d_h}. \quad (24)$$

417 Now we link this to \mathbf{L} by using that

$$\mathbf{L}^{\text{nloc}} = \left(-\alpha \nabla_N^{\text{nloc}} \Theta + \beta \nabla_N^{\text{nloc}} S_A \right) \neq 0, \quad (25)$$

⁴¹⁸ implying that there is a change in ρ along the approximate NTP given by

$$\Delta\rho = \rho \left| \mathbf{L}^{\text{nloc}} \right| d_h. \quad (26)$$

⁴¹⁹ Here $\Delta\rho$ can be interpreted as the density difference over the finite-difference NTP. Using that
⁴²⁰ $N^2 \approx -(g/\rho)(\Delta\rho/\Delta z)$, this $\Delta\rho$ can then be related to the 'vertical distance' Δz that one needs
⁴²¹ to move in order to find such a ρ change. Because $\Delta\rho$ is the density difference between the
⁴²² approximate and exact NTP, the related Δz can be interpreted as an approximate height difference
⁴²³ between the approximate and exact NTP, which is the same as Δz_ε , leaving:

$$\Delta z_\varepsilon = -g d_h \frac{\left| \mathbf{L}^{\text{nloc}} \right|}{N^2}, \quad \rightarrow \quad D_f^{\text{nloc}} = K g^2 \frac{\left| \mathbf{L}^{\text{nloc}} \right|^2}{N^4}. \quad (27)$$

⁴²⁴ Where we used Eqs. (23) - (26) to obtain the second part. By replacing \mathbf{L}^{nloc} with one obtained
⁴²⁵ using gradients from the other methods, we can calculate D_f^{local} , D_f^{hybrid} and $D_f^{\sigma_2}$.

⁴²⁶ In the ocean, a small-scale diffusivity of $D = \mathcal{O}(10^{-5} \text{ m}^2 \text{ s}^{-1})$ is considered to be "background"
⁴²⁷ mixing (Waterhouse et al. 2014). A D_f that exceeds the background mixing adds significant un-
⁴²⁸ physical ocean mixing to calculations. The resulting distribution for D_f (Fig. 6), shows that for the
⁴²⁹ non-local method 3.1% of the grid-points have a value for which $D_f > 10^{-5}$. In contrast, for the
⁴³⁰ hybrid-method (20.3%), the local-method (22 %) and σ_2 (23 %), about 1 in every five T-grid points
⁴³¹ exceed $D_f = 10^{-5} \text{ m}^2 \text{ s}^{-1}$. For the non-local method these few locations are located at hot-spots
⁴³² in the Southern Ocean, while larger values for D_f are more spread out for the other methods.

⁴³³ The non-local method is here based on satisfying $\Delta v \leq v_{\text{crit}}$ (Eq. 21) rather than satisfying the
⁴³⁴ neutral condition of $\alpha \nabla_N \Theta = \beta \nabla_N S_A$ (Eq. 22). Except for the limits of numerical precision, and
⁴³⁵ the limits set by step 2 of the search algorithm (section 3b2), one could argue that D_f^{nloc} should be
⁴³⁶ zero. As shown in Appendix A of Jackett and McDougall (1997) however, satisfying $\Delta v \leq v_{\text{crit}}$
⁴³⁷ is only approximately the same as satisfying $\alpha \nabla_N \Theta = \beta \nabla_N S_A$. In this study, we assessed the
⁴³⁸ neutrality of D_f^{nloc} by means of $\alpha \nabla_N \Theta = \beta \nabla_N S_A$, while the algorithm determines this neutrality

439 by means of satisfying $\Delta v \leq v_{\text{crit}}$. As this is not exactly the same, this leads to non-zero values of
 440 D_f^{nloc} that are unrelated to the accuracy of the algorithm, but related to the method of assessment.
 441 D_f^{nloc} may therefore be more accurate than shown in Fig. 6.

442 *e. Cabbeling and thermobaricity*

443 A globally integrated quantitative measure of the effect of the differences in neutral gradients on
 444 ocean physics can be obtained by calculating the water mass transformation (WMT, Walin 1982;
 445 Groeskamp et al. 2019) due to cabbeling and thermobaricity. Cabbeling and thermobaricity result
 446 from the fact that Θ and S_A can mix along neutral surfaces, but that the density of the resulting
 447 mixture is a nonlinear function of Θ , S_A and P and may no longer be the same as the original den-
 448 sity (Witte 1902; Foster 1972; McDougall 1984, 1987b). Neutral diffusion along curved density
 449 isolines leads to a dianeutral transport that can be quantified in terms of WMT (Marsh 2000; Talley
 450 and Yun 2001; Iudicone et al. 2008; Urakawa and Hasumi 2012; Groeskamp et al. 2016, 2017).
 451 Here the WMT due to cabbeling (T_{cab}) and thermobaricity (T_{thb}) in Neutral Density coordinates is
 452 given by (Iudicone et al. 2011; Groeskamp et al. 2016):

$$T_{\text{Cab}}(\gamma^n) = -\frac{\partial}{\partial \gamma^n} \int_{V(\gamma_*^n \leq \gamma^n)} -K b \gamma^n C_b |\nabla_N \Theta|^2 dV, \quad (28)$$

$$T_{\text{Thb}}(\gamma^n) = -\frac{\partial}{\partial \gamma^n} \int_{V(\gamma_*^n \leq \gamma^n)} -K b \gamma^n T_b \nabla_N P \cdot \nabla_N \Theta dV. \quad (29)$$

453 Here $\int_{V(\gamma_*^n \leq \gamma^n)} dV$ is the integral over the volume for which $\gamma_*^n \leq \gamma^n$, such that $T_{\gamma^n}(\gamma^n)$ is the
 454 WMT of γ^n into a larger density. For the diffusivity we used $K = 1000 \text{ m}^2 \text{ s}^{-1}$. Positive (negative)
 455 values indicate transformation into denser (lighter) water (Fig. 8). The dimensionless ratio $b =$
 456 $|\nabla \gamma| / |\nabla \rho_l|$ results from the definition of γ^n (Jackett and McDougall 1997). Here ρ_l is the locally
 457 referenced potential density, C_b and T_b are the cabbeling and thermobaricity coefficients as defined
 458 by McDougall (1984, 1987a). The WMT rates (in Sv, where $1 \text{ Sv} = 10^6 \text{ m}^3 \text{ s}^{-1}$) are calculated and

459 binned using monthly means. By replacing $\nabla_N\Theta$ and ∇_NS_A in Eqs. (28)-(29) with those obtained
460 by the different methods, their respective WMT rates are obtained ($T_{\text{Cab}}^{\text{nloc}}$, $T_{\text{Cab}}^{\text{local}}$, $T_{\text{Cab}}^{\text{hybrid}}$, and $T_{\text{Cab}}^{\sigma_2}$,
461 and the same for T_{Thb}).

462 The WMT due to cabbeling using neutral gradients from the local-method or σ_2 , leads to trans-
463 port of 134 and 164 Sv, respectively. This is of the same magnitude as estimates of the Antarctic
464 Circumpolar Current (134-174 Sv, Whitworth and Peterson 1985; Donohue et al. 2016). Such
465 amounts of cabbeling would produce large amounts of water of a $\gamma^n \approx 28.25 \text{ kg m}^{-3}$, of which
466 there is no indication from the observed ocean's stratification. There is also no known mixing, air-
467 sea flux or geothermal heating effect that compensates this production (de Lavergne et al. 2015;
468 Groeskamp et al. 2017).

469 Using an isopycnal model, Marsh (2000) finds annual mean WMT with maximum values of
470 about 10 Sv for the Southern Ocean. Klocker and McDougall (2010) used state of the art accurate
471 and smooth representation of neutral surfaces (ω -surfaces, Klocker et al. 2009), applied to an
472 annual mean climatology (WOCE, Viktor Gouretski and K. P. Koltermann 2004) to find about
473 5 Sv of cabbeling and 1 Sv of Thermobaricity. The non-local and hybrid method have cabbeling
474 maxima of 22 Sv and 26 Sv, respectively. These results are likley higher because Marsh (2000)
475 is not global, the study of Klocker and McDougall (2010) is performed on annual means, while
476 all studies use different values for K . From these estimates and Fig. 8, we conclude that, as
477 applied in this study, the local-method produces a physically unrealistic amount of cabbeling and
478 thermobaricity, while the non-local and hybrid method produce results that are physically realistic.
479 However, note that both the cabbeling and thermobaricity estimates of the non-local method and
480 hybrid-method still show significant differences, with even a sign difference for thermobaricity for
481 some densities.

482 *f. Comparing Vertical Heat Transport*

483 The last measure we employ to illustrate and quantify the differences between the methods is
 484 by means of calculating the heat flux by neutral diffusion. We can project the neutral flux into the
 485 lateral and vertical directions and integrate spatially to obtain the corresponding meridional and
 486 vertical eddy heat transports:

$$H(y) = -Kc_p^0 \iint \rho \nabla_N \Theta \cdot \hat{\mathbf{j}} \, dx \, dz \quad H(z) = \underbrace{\int \left[-Kc_p^0 \int \rho \nabla_N \Theta \cdot \hat{\mathbf{k}} \, dx \right] dy}_{h(y,z)} \quad (30)$$

487 with the heat capacity of seawater c_p^0 ($\text{J kg}^{-1} \text{ K}^{-1}$). Here $h(y,z)$ is the heat transport per meter
 488 latitude (W m^{-1}), such that $H(z)$ is the integrated global vertical heat transport (W). By substitut-
 489 ing $\nabla_N \Theta$ in Eq. (30) with neutral gradients obtained by the different methods, the respective heat
 490 transport estimates are obtained.

491 The peak meridional heat transports change 25% using the local-method compared to the non-
 492 local method (for latitude 50°S and 40°N, panel A, Fig. 9), while the local-method sometimes has
 493 the opposite sign to the non-local method (for latitude 40°S). In addition we find strong differences
 494 in the magnitude and sign of the estimates of $h(y,z = 1000)$ (panel B, Fig. 9), which holds when
 495 globally integrated and for many different depths (panel C, Fig. 9). Fig. 7 of Gregory (2000)
 496 shows the vertical heat transport of the HadCM2 atmosphere-ocean general circulation model
 497 (AOGCM) and has a comparable structure to that of the non-local and hybrid method (panel C,
 498 Fig. 9). That is, a subsurface peak with positive values in about the first 1500 m of the column
 499 and small negative values below that. Their maximum value is up to 4 W m^{-2} , whereas that of the
 500 non-local method is about 1.5 W m^{-2} .

501 Notably, the local method produces a much stronger mid-themocline downward heat flux than
 502 the other three methods. The fact that the magnitude and even direction of the inferred vertical

503 heat transport depends so strongly on the method used to calculate neutral gradients means that
504 this issue has relevance for the large scale ocean circulation and climate.

505 5. Conclusion

506 In this paper, we presented a new (vertically) non-local method to calculate neutral slopes and
507 tracer gradients applicable to gridded data sets and numerical ocean simulations. We compared the
508 non-local approach (based on a search algorithm) with more traditional local-approaches (based
509 on a local grid stencil).

510 The local-method is based on calculating neutral slopes and tracer gradients using a local grid
511 stencil. This method suffers from numerical issues that lead to *ad hoc* regularization methods that
512 strongly influence the results. The non-local method is based on an approximate expression for
513 calculating NTPs that is satisfied using a non-local searching algorithm. The non-local method
514 requires no regularization beyond that naturally defined by the grid resolution. We also introduced
515 the hybrid-method for use in testing the non-local method. The hybrid method uses the neutral
516 slopes from the non-local method combined with Cartesian tracer gradients based on the local
517 grid-stencil to calculate neutral tracer gradients. We used a gridded climatology to test the non-
518 local method as compared to the other methods. Our results show that the non-local method
519 reduces fictitious diffusivity and produces more plausible estimates for water mass transformation
520 and vertical heat transport. Additionally, the hybrid method suffers from numerical issues arising
521 from local extremes that are produced when calculating Cartesian tracer gradients using the local
522 grid stencil.

523 Isopycnal layered models typically make use of potential density referenced to 2000 dbar, σ_2 ,
524 to estimate neutral surfaces. Our results suggest that when gradients of Θ , S_A and P are calcu-
525 lated based on a searching algorithm (as for the non-local method, but along σ_2 surfaces), water

526 mass transformation, heat transport and fictitious diffusivities are comparable in magnitude to that
527 of the local-method. This result suggests that layered ocean models need to find more accurate
528 representation of neutral directions than the σ_2 surfaces typically used.

529 Implementing the non-local method may also influence other variables than those presented in
530 this study, including parameterized eddy-induced advective transport as per the Gent et al. (1995)
531 scheme that is commonly used in mesoscale inactive climate models. It has been shown that
532 changing the tracer fluxes ($-K\nabla_N C$) by means of changing the mesoscale diffusivity K has large
533 impact on the climate (Pradal and Gnanadesikan 2014). Here, instead of changing K , the flux is
534 improved by having a more accurate representation of the neutral gradients $\nabla_N C$. Based on the
535 nontrivial sensitivities found here, we conjecture that improving the calculation for neutral gradi-
536 ents will have a significant impact on numerical climate simulations. Furthermore, the non-local
537 method as provided in this study is computationally more expensive than the local-method. How-
538 ever, Shao et al. (in prep) propose a non-local method based on the same principles proposed here
539 yet using a computationally efficient method suitable for ocean modeling. This model implemen-
540 tation will in turn facilitate the testing of prognostic simulations using the more accurate neutral
541 slope calculation proposed here.

542 *Acknowledgments.* SG and RPA acknowledge support from NASA Award NNX14AI46. SG,
543 PMB and TJM acknowledges support from the Australian Research Council Grant FL150100090.
544 We thank Andrew Shao for useful discussion on this subject.

APPENDIX A

546 **A1. The new algorithm**

547 The algorithm is designed for a z-coordinate tracer grid (T-grid). The tracer C is defined over
 548 the T-grid, with grid center at (x_i, y_j, z_k) so that $C_{i,j,k} = C(x_i, y_j, z_k)$ (Fig. 10). Here $i = 1, 2, \dots, I$,
 549 where I is the total number of discrete longitude locations. In a similar way j and J represent
 550 latitude locations, k and K represent depths. A T-grid cell has volume $V_{i,j,k} = dx dy dz$, where
 551 $dx = x_{j,i+\frac{1}{2}} - x_{j,i-\frac{1}{2}}$ and $dy = y_{j+\frac{1}{2}} - y_{j-\frac{1}{2}}$, and $dz = z_{k+\frac{1}{2}} - z_{k-\frac{1}{2}}$. Note that the ' $+\frac{1}{2}$ ' indicates
 552 a position at an interface between two T-grid points and that dx is a function of latitude. $V_{i,j,k}$ is
 553 enclosed by 6 interfaces (two in each X , y and z direction). Here is the notation of three such areas
 554 (one in each direction) of whose areas are

$$\begin{aligned} 555 \quad A_{yz}(i + \frac{1}{2}, j, k) &= A_{yz}(x_{i+\frac{1}{2}}, y_j, z_k) = dy dz \\ 556 \quad A_{xz}(i, j + \frac{1}{2}, k) &= A_{xz}(x_i, y_{j+\frac{1}{2}}, z_k) = dx dz \\ 557 \quad A_{xy}(i, j, k + \frac{1}{2}) &= A_{xy}(x_i, y_j, z_{k+\frac{1}{2}}) = dx dy. \end{aligned} \quad (\text{A1})$$

558 The algorithm provides neutral tracer gradients and neutral slopes on predetermined gridpoints at
 559 the T-cell interfaces. There are two main steps to the algorithm: 1) - iteration to find a neutral
 560 surface, and 2) iteration to find the neutral surface that crosses through the pre-determined vertical
 561 grid-point.

562 *a. Step 1: Finding a neutral tangent plane.*

563 We start by constructing an NTP from a south cast (x_i, y_j, z_k) to a north cast (x_i, y_{j+1}, z_k) . As the
 564 NTP is only defined locally, the reference pressure defines where the tracer gradients and neutral
 565 slopes are estimated. We start with the following steps:

- 566 1. Define $\Theta_{\text{south}} = \Theta_{i,j,k}$ and $\Theta_{\text{north}} = \Theta_{i,j+1,k-1}$, with Θ_{north} one grid-point deeper than Θ_{south}
 567 (the same for S_A , P and other tracers). This allows us to define the mid-pressure $P_m = 0.5 \times$

568 $(P_{\text{south}} + P_{\text{north}})$ and calculate $\Delta v = v(S_{A,\text{north}}, \Theta_{\text{north}}, P_m) - v(S_{A,\text{south}}, \Theta_{\text{south}}, P_m) \leq v_{\text{crit}}$ as
569 in equation (20).

- 570 2. If $|\Delta v| \not\leq v_{\text{crit}}$, we use linear vertical interpolation to find a new pressure with new values
571 for $S_{A,\text{north}}$, Θ_{north} , and P_{north} such that $|\Delta v| \leq v_{\text{crit}}$, while keeping $S_{A,\text{south}}$, Θ_{south} and P_{south}
572 fixed. We have implicitly assumed that S_A and Θ vary linearly with P on each vertical cast.
573 If no position is found where the criteria $|\Delta v| \not\leq v_{\text{crit}}$ is satisfied, then a NaN (Not a Number)
574 is returned.

575 The NTP is estimated by the straight line that connects the the south-cast (x_i, y_j, z_k) with the north-
576 cast $(x_i, y_{j+1}, z_{\text{north}})$. However, due to the vertical interpolation z_{north} will generally not be at the
577 center of a T-grid. Resulting tracer gradients and neutral slopes in turn would not be given at P_m ,
578 which is unlikely to be exactly at $A_{xz}(i, j + \frac{1}{2}, k)$ (the middle of the interface). Although this offset
579 may be fine for some applications, for many studies it is preferred to have the neutral gradients
580 and tracer slopes at the middle of the T-cell interfaces. Therefore, the next step iteratively moves
581 the north and south intersection of the NTP with the cast, up and down the cast, to find a NTP that
582 crosses exactly through the middle of the A_{xz} interface.

583 Code to implement Step 1 is available at <http://www.teos-10.org> as part of the gsw-software
584 package (McDougall and Barker 2011) under the name “*gsw_ntp_bottle_to_cast_gradients*”.

585 *b. Step 2: Finding the neutral tangent plane at a target pressure.*

586 We define the target pressure $P_{\text{target}} = P_{i,j+\frac{1}{2},k}$ through which we wish the NTP to cross, and
587 we seek a revised value of P_m that satisfies $|\Delta P| = |P_{\text{target}} - P_m| \leq P_{\text{crit}} = 0.1$ dbar. We use the
588 following steps to find a NTP that satisfies this criteria.

589 1. Calculate and subtract ΔP from P_{south} using

$$P_{\text{new}} = P_{\text{south}} - f(n)\Delta P, \quad \text{with} \quad f(n) = \begin{cases} 1 & n \leq n_0 \\ e^{a(n-n_0)} & n_0 < n \leq n_{\text{max}}. \end{cases} \quad (\text{A2})$$

590 Here $f(n)$ is relaxation factor that changes for each iteration, n ; $n_0 = 2$; $n_{\text{max}} = 10$ and the ex-
591 ponential constant $a = -0.0461$ is numerically tuned to speed up the iterative process. Using
592 linear, vertical interpolation, new values for $S_{A,\text{new}}$ and Θ_{new} are determined at P_{new} . Subse-
593 quently, starting from $(S_{A,\text{new}}, \Theta_{\text{new}}, P_{\text{new}})$, we find a new NTP using the method described in
594 Appendix 5a. Eventually, this provides a new P_m from which we calculate a new ΔP . This
595 process is repeated n times, until we find that $|\Delta P| \leq 0.5$ dbar, and use $f(n)$ to help reduce
596 the number of iterations required.

597 2. The above procedure is simultaneously applied from south to north and from north to south.
598 The first solution from either direction that satisfies $|\Delta P| \leq 0.5$ dbar is used as the solution.
599 If surfaces incrop or outcrop and no solution is found, then NaN is returned. If a solution
600 is found, but not within the criteria, we save the index and approximate the solution with a
601 different routine (Step 3, below).

602 The routine above provides us with a NTP that will move through the required target pressure with
603 a 50 cm accuracy.

604 c. *Step 3: Calculating the Slopes and the Gradients.*

605 Using the NTP constructed in the previous two steps, we now define our final values for $\Theta_{\text{south}} =$
606 $\Theta(x_i, y_j, k_{\text{south}})$, and $\Theta_{\text{north}} = \Theta(x_i, y_j, k_{\text{north}})$ and in a similar way also for S_A and P . We use the
607 following steps to calculate the tracer gradients in the north-south direction.

608 3a After calculating z_{north} and z_{south} from P_{north} and P_{south} we can calculate $\Delta z = z_{\text{north}} - z_{\text{south}}$,
 609 $\Delta y = y_{\text{north}} - y_{\text{south}}$ and subsequently $S_y^{\text{nloc}} = \frac{\Delta z}{\Delta y}$. The neutral Θ gradient can be calculated as

$$\nabla_N^{\text{nloc}} \Theta \cdot \hat{\mathbf{y}} = \frac{\Delta \Theta|_{N,x}}{\Delta y} = \frac{\Theta_{\text{north}} - \Theta_{\text{south}}}{\Delta y}. \quad (\text{A3})$$

610 Neutral gradients for S_A and P are obtained in a similar manner.

611 3b We now vertically interpolate using all available values of $\nabla_N^{\text{nloc}} \Theta \cdot \hat{\mathbf{y}}$ on a vertical cast to find
 612 the gradients at P_{target} for locations where the NTP did not outcrop or incrop, but could not
 613 iterate within the criteria (see step 2.2 of the previous section). The values provided near but
 614 not within the limit of P_{target} are used and replaced in this process. The vertical interpolation
 615 is generally over small distances. Hence, effects of the nonlinear equation of state that are
 616 not taken into account should be small. The remaining locations that have no allocated values
 617 (e.g., outcrops set to NaN) are interpolated using the Matlab natural nearest neighbor interpola-
 618 tion, and extrapolated using nearest neighbor. Both choices are motivated to avoid creating
 619 extremes.

620 3c Step 1 (section 5a), Step 2 (section 5b) and step 3a and 3b are repeated for the East-West
 621 direction, providing $\nabla_N^{\text{nloc}} \Theta \cdot \hat{\mathbf{x}} = \Delta \Theta|_{N,y} / \Delta x = (\Theta_{\text{east}} - \Theta_{\text{west}}) / (x_{\text{east}} - x_{\text{west}})$, leaving all the
 622 variables required to obtain neutral gradients in both the south-north and east-west direction.
 623 To obtain $\nabla_N \Theta \cdot \hat{\mathbf{z}}$ however, a few more steps were required.

624 3d Here $\nabla_N \Theta \cdot \hat{\mathbf{z}}$ needs to be provided at $(x_i, y_j, k + \frac{1}{2})$. We therefore vertically averaged the tracers
 625 at the T-grids to obtain $\Theta_{i,j,k+\frac{1}{2}}$, and similarly for S_A and P . Simultaneously to calculate the
 626 NTP and related gradients for the tracers starting at the k locations, we also calculate them
 627 for $k + \frac{1}{2}$ locations. This provides slopes and gradients at the location $P(x_i, y + \frac{1}{2}, k + \frac{1}{2})$ (at
 628 the middle of the interface and between two vertical grid point). At these location we then

629 calculate $S_x \frac{\Delta C|_{N,y}}{\Delta x}$ or $S_y \frac{\Delta C|_{N,x}}{\Delta y}$. These values are then averaged horizontally and then summed
630 up (Eq. 18) to obtain $\nabla_N \Theta \cdot \hat{z}$.

631 The algorithm described above provides neutral slopes and gradients (Eq. 18). As described
632 above, we use two main steps, 1) finding the NTP, and 2) finding the NTP at the right pressure.
633 There is no reason why these two could not be combined into a version that might iterate faster
634 and perform better, based on a combined criteria. However, that is beyond the scope of this study.
635 Finally, the slopes of the σ_2 surfaces in WOA, and related tracer gradients are also obtained using
636 a search algorithm, comparable to the direct method. A similar type algorithm is also described in
637 the Appendix of Groeskamp et al. (2016) for Neutral Density.

638 References

- 639 Abernathey, R. P., and J. Marshall, 2013: Global surface eddy diffusivities derived from satellite al-
640 timetry. *Journal of Geophysical Research: Oceans*, **118** (2), 901–916, doi:10.1002/jgrc.20066.
- 641 Barker, P. M., and T. J. McDougall, 2017: Stabilizing hydrographic profiles with minimal change
642 to the water masses. *Journal of Atmospheric and Oceanic Technology*, **34** (9), 1935–1945, doi:
643 10.1175/JTECH-D-16-0111.1.
- 644 Bleck, R., 1978a: Finite difference equations in generalized vertical coordinates, I, Total energy
645 conservation. *Contrib. Atmos. Phys.*, **51**, 360–372.
- 646 Bleck, R., 1978b: Finite difference equations in generalized vertical coordinates, II, Potential
647 vorticity conservations. *Contrib. Atmos. Phys.*, **52**, 95–105.
- 648 Boyer, T., and Coauthors, 2013: World Ocean Database 2013, NOAA Atlas NESDIS 72.
649 <http://doi.org/10.7289/V5NZ85MT>, 209 pp.

- 650 Cole, S. T., C. Wortham, E. Kunze, and W. B. Owens, 2015: Eddy stirring and horizontal dif-
651 fusivity from argo float observations: Geographic and depth variability. *Geophysical Research*
652 *Letters*, **42** (10), 3989–3997, doi:10.1002/2015GL063827.
- 653 Cox, M. D., 1987: Isopycnal diffusion in a z -coordinate ocean model. *Ocean Modelling*, **74**, 1–5.
- 654 Danabasoglu, G., R. Ferrari, and J. McWilliams, 2008: Sensitivity of an ocean general circulation
655 model to a parameterization of near-surface eddy fluxes. *Journal of Climate*, **21**, 1192–1208.
- 656 Danabasoglu, G., and J. C. McWilliams, 1995: Sensitivity of the global ocean circulation to pa-
657 rameterizations of mesoscale tracer transports. *Journal of Climate*, **8**, 2967–2987.
- 658 de Lavergne, C., G. Madec, J. Le Sommer, A. J. G. Nurser, and A. C. Naveira Garabato, 2015: On
659 the consumption of Antarctic Bottom Water in the abyssal ocean. *Journal of Physical Oceanog-
660 raphy*, doi:10.1175/JPO-D-14-0201.1.
- 661 Donohue, K. A., K. L. Tracey, D. R. Watts, M. P. Chidichimo, and T. K. Chereskin, 2016: Mean
662 antarctic circumpolar current transport measured in drake passage. *Geophysical Research Let-
663 ters*, **43** (22), 11,760–11,767, doi:10.1002/2016GL070319.
- 664 Ferrari, R., S. M. Griffies, A. J. G. Nurser, and G. K. Vallis, 2010: A boundary-value problem for
665 the parameterized mesoscale eddy transport. *Ocean Modelling*, **32**, 143–156.
- 666 Ferrari, R., J. C. McWilliams, V. M. Canuto, and M. Dubovikov, 2008: Parameterization of
667 eddy fluxes near oceanic boundaries. *Journal of Climate*, **21** (12), 2770–2789, doi:10.1175/
668 2007JCLI1510.1.
- 669 Foster, T. D., 1972: An analysis of the cabbeling instability in sea water. *Journal of Physical
670 Oceanography*, **2** (3), 294–301, doi:10.1175/1520-0485(1972)002<0294:AAOTCI>2.0.CO;2.

- 671 Fox-Kemper, B., R. Lumpkin, and F. Bryan, 2013: Lateral transport in the ocean interior. *Ocean*
672 *Circulation and Climate, 2nd Edition: A 21st Century Perspective*, G. Siedler, S. M. Griffies,
673 J. Gould, and J. Church, Eds., International Geophysics Series, Vol. 103, Academic Press, 185–
674 209.
- 675 Gent, P. R., and J. C. McWilliams, 1990: Isopycnal Mixing in Ocean Circulation Models. *Jour-*
676 *nal of Physical Oceanography*, **20** (1), 150–155, doi:10.1175/1520-0485(1990)020\$(\$0150:
677 IMIOCM\$)\$2.0.CO;2, URL [http://dx.doi.org/10.1175/1520-0485\(1990\)020\\$\(\\$0150:IMIOCM\\$\)2.0.CO;2](http://dx.doi.org/10.1175/1520-0485(1990)020$($0150:IMIOCM$)2.0.CO;2).
- 678 Gent, P. R., J. Willebrand, T. J. McDougall, and J. C. McWilliams, 1995: Parameterizing Eddy-
679 Induced Tracer Transports in Ocean Circulation Models. *Journal of Physical Oceanography*,
680 **25** (4), 463–474, doi:10.1175/1520-0485(1995)025\$(\$0463:PEITTI\$)\$2.0.CO;2.
- 681 Gerdes, R., C. Köberle, and J. Willebrand, 1991: The influence of numerical advection schemes
682 on the results of ocean general circulation models. *Climate Dynamics*, **5**, 211–226.
- 683 Gnanadesikan, A., 1999: A global model of silicon cycling: Sensitivity to eddy parameterization
684 and dissolution. *Global Biogeochemical Cycles*, **13** (1), 199–220.
- 685 Gnanadesikan, A., S. M. Griffies, and B. L. Samuels, 2007: Effects in a climate model of slope
686 tapering in neutral physics schemes. *Ocean Modelling*, **17**, 1–16.
- 687 Gnanadesikan, A., M.-A. Pradal, and R. Abernathey, 2015: Isopycnal mixing by mesoscale ed-
688 dies significantly impacts oceanic anthropogenic carbon uptake. *Geophysical Research Letters*,
689 **42** (11), 4249–4255, doi:10.1002/2015GL064100.

- 691 Graham, F. S., and T. J. McDougall, 2013: Quantifying the Nonconservative Production of Con-
692 servative Temperature, Potential Temperature, and Entropy. *Journal of Physical Oceanography*,
693 **43** (5), 838–862, doi:10.1175/JPO-D-11-0188.1.
- 694 Gregory, J. M., 2000: Vertical heat transports in the ocean and their effect on time-dependent
695 climate change. *Climate Dynamics*, **16** (7), 501–515, doi:10.1007/s003820000059.
- 696 Griffies, S., and Coauthors, 2005: Formulation of an ocean model for global climate simulations.
697 *Ocean Science*, **1** (1), 45–79.
- 698 Griffies, S. M., 1998: The Gent–McWilliams Skew Flux. *Journal of Physical Oceanography*,
699 **28** (5), 831–841, doi:10.1175/1520-0485(1998)028<0831:TGMSF>2.0.CO;2.
- 700 Griffies, S. M., 2004: *Fundamentals of ocean climate models*. Princeton University Press.
- 701 Griffies, S. M., 2012: Elements of the modular ocean model (mom). *NOAA Geophysical Fluid
702 Dynamics Laboratory, Princeton, USA*.
- 703 Griffies, S. M., A. Gnanadesikan, R. C. Pacanowski, V. Larichev, J. K. Dukowicz, and R. D. Smith,
704 1998: Isoneutral diffusion in a z -coordinate ocean model. *Journal of Physical Oceanography*,
705 **28**, 805–830.
- 706 Groeskamp, S., R. P. Abernathey, and A. Klocker, 2016: Water mass transformation by cabling
707 and thermobaricity. *Geophysical Research Letters*, doi:10.1002/2016GL070860.
- 708 Groeskamp, S., S. M. Griffies, D. Iudicone, R. Marsh, A. J. G. Nurser, and J. D. Zika, 2019: The
709 water mass transformation framework for ocean physics and biogeochemistry. *Annu. Rev. Mar.
710 Sci.*, **11**, doi:<https://doi.org/10.1146/annurev-marine-010318-095421>.

- 711 Groeskamp, S., B. M. Sloyan, J. D. Zika, and T. J. McDougall, 2017: Mixing inferred from an
712 ocean climatology and surface fluxes. *Journal of Physical Oceanography*, **47** (3), 667–687,
713 doi:10.1175/JPO-D-16-0125.1.
- 714 Hirst, A. C., D. R. Jackett, and T. J. McDougall, 1996: The Meridional Overturning Cells of a
715 World Ocean Model in Neutral Density Coordinates. *Journal of Physical Oceanography*, **26** (5),
716 775–791, doi:10.1175/1520-0485(1996)026\$(\$0775:TMOCOA\$)\$2.0.CO;2.
- 717 IOC, SCOR, and IAPSO, 2010: *The international thermodynamic equation of seawater – 2010:*
718 *Calculation and use of thermodynamic properties*. [Available online at www.TEOS-10.org],
719 Intergovernmental Oceanographic Commission, Manuals and Guides. UNESCO (English).
- 720 Iselin, C. O., 1939: The influence of vertical and lateral turbulence on the characteristics of the
721 waters at mid-depths. *Eos, Transactions American Geophysical Union*, **20** (3), 414–417, doi:
722 10.1029/TR020i003p00414.
- 723 Iudicone, D., G. Madec, and T. J. McDougall, 2008: Water-Mass Transformations in a Neutral
724 Density Framework and the Key Role of Light Penetration. *Journal of Physical Oceanography*,
725 **38** (7), 1357–1376, doi:10.1175/2007JPO3464.1.
- 726 Iudicone, D., K. B. Rodgers, I. Stendardo, O. Aumont, G. Madec, L. Bopp, O. Mangoni, and
727 M. Ribera d'Alcalá, 2011: Water masses as a unifying framework for understanding the South-
728 ern Ocean carbon cycle. *Biogeosciences*, **8** (5), 1031–1052, doi:10.5194/bg-8-1031-2011, URL
729 <http://www.biogeosciences.net/8/1031/2011/>.
- 730 Jackett, D. R., and T. J. McDougall, 1997: A Neutral Density Variable for the World's Oceans.
731 *Journal of Physical Oceanography*, **27** (2), 237–263, doi:10.1175/1520-0485(1997)027<0237:
732 ANDVFT>2.0.CO;2.

- 733 Klocker, A., and R. Abernathey, 2013: Global Patterns of Mesoscale Eddy Properties and Diffu-
734 sivities. *Journal of Physical Oceanography*, **44** (3), 1030–1046, doi:10.1175/JPO-D-13-0159.1.
- 735 Klocker, A., and T. J. McDougall, 2010: Influence of the nonlinear equation of state on global
736 estimates of dianeutral advection and diffusion. *Journal of Physical Oceanography*, **40** (8),
737 1690–1709, doi:10.1175/2010JPO4303.1, URL <http://dx.doi.org/10.1175/2010JPO4303.1>.
- 738 Klocker, A., T. J. McDougall, and D. R. Jackett, 2009: A new method for forming approximately
739 neutral surfaces. *Ocean Science*, **5** (2), 155–172, doi:10.5194/os-5-155-2009.
- 740 Lemarié, F., L. Debreu, A. F. Shchepetkin, and J. C. McWilliams, 2012: On the stability and
741 accuracy of the harmonic and biharmonic isoneutral mixing operators in ocean models. *Ocean
742 Modelling*, **52-53**, 9–35.
- 743 Madec, G., 2015: NEMO ocean engine.
- 744 Marsh, R., 2000: Cabbeling due to isopycnal mixing in isopycnic coordinate models. *Journal of
745 Physical Oceanography*, **30** (7), 1757–1775, doi:10.1175/1520-0485(2000)030<1757:CDTIMI>
746 2.0.CO;2.
- 747 Marshall, J., A. Adcroft, C. Hill, L. Perelman, and C. Heisey, 1997: A finite-volume, incompress-
748 ible navier stokes model for studies of the ocean on parallel computers. *Journal of Geophysical
749 Research: Oceans*, **102** (C3), 5753–5766, doi:10.1029/96JC02775.
- 750 Marshall, J., J. R. Scott, A. Romanou, M. Kelley, and A. Leboissetier, 2017: The dependence of
751 the ocean’s moc on mesoscale eddy diffusivities: A model study. *Ocean Modelling*, **111**, 1–8,
752 doi:<https://doi.org/10.1016/j.ocemod.2017.01.001>.
- 753 McDougall, T., and P. M. Barker, 2011: *Getting started with TEOS-10 and the Gibbs Seawater
754 (GSW) Oceanographic Toolbox*. WG127, ISBN 978-0-646-55621-5, SCOR/IAPSO.

- 755 McDougall, T. J., 1984: The Relative Roles of Diapycnal and Isopycnal Mixing on Subsurface
756 Water Mass Conversion. *Journal of Physical Oceanography*, **14** (10), 1577–1589, doi:10.1175/
757 1520-0485(1984)014<1577:TRRODA>2.0.CO;2.
- 758 McDougall, T. J., 1987a: Neutral Surfaces. *Journal of Physical Oceanography*, **17** (11), 1950–
759 1964, doi:10.1175/1520-0485(1987)017<1950:NS>2.0.CO;2.
- 760 McDougall, T. J., 1987b: Thermobaricity, cabbeling, and water-mass conversion. *Journal of Geo-*
761 *physical Research: Oceans*, **92** (C5), 5448–5464, doi:10.1029/JC092iC05p05448.
- 762 McDougall, T. J., 2003: Potential Enthalpy: A Conservative Oceanic Variable for Evaluating Heat
763 Content and Heat Fluxes. *Journal of Physical Oceanography*, **33** (5), 945–963, doi:10.1175/
764 1520-0485(2003)033<0945:PEACOV>2.0.CO;2.
- 765 McDougall, T. J., and J. A. Church, 1986: Pitfalls with the Numerical Representation of Isopyc-
766 nal Diapycnal Mixing. *Journal of Physical Oceanography*, **16** (1), 196–199, doi:10.1175/
767 1520-0485(1986)016<0196:PWTNRO>2.0.CO;2.
- 768 McDougall, T. J., S. Groeskamp, and S. M. Griffies, 2014: On geometrical aspects of in-
769 terior ocean mixing. *Journal of Physical Oceanography*, **44** (8), 2164–2175, doi:10.1175/
770 JPO-D-13-0270.1.
- 771 McDougall, T. J., and D. R. Jackett, 1988: On the helical nature of neutral trajectories in the ocean.
772 *Progress In Oceanography*, **20** (3), 153 – 183, doi:DOI:10.1016/0079-6611(88)90001-8.
- 773 McDougall, T. J., and D. R. Jackett, 2005: The material derivative of neutral density. *Journal of*
774 *Marine Research*, **63** (1), 159–185, doi:doi:10.1357/0022240053693734.
- 775 McDougall, T. J., and D. R. Jackett, 2009: *Neutral surfaces and the equation of state*, 4097 –
776 4103. Elsevier.

- 777 McDougall, T. J., and P. C. McIntosh, 2001: The Temporal-Residual-Mean Velocity. Part II: Isopyc-
778 nal Interpretation and the Tracer and Momentum Equations. *Journal of Physical Oceanogra-*
779 *phy*, **31** (5), 1222–1246, doi:10.1175/1520-0485(2001)031<1222:TTRMVP>2.0.CO;2.
- 780 Olbers, D. J., M. Wenzel, and J. Willebrand, 1986: The inference of north atlantic circulation
781 patterns from climatological hydrographic data. *Reviews of Geophysics*, **23** (4), 313–356, doi:
782 10.1029/RG023i004p00313.
- 783 Pradal, M.-A., and A. Gnanadesikan, 2014: How does the redi parameter for mesoscale mixing
784 impact global climate in an earth system model? *Journal of Advances in Modeling Earth Sys-*
785 *tems*, **6** (3), 586–601, doi:10.1002/2013MS000273.
- 786 Redi, M. H., 1982: Oceanic Isopycnal Mixing by Coordinate Rotation. *Journal of Physical*
787 *Oceanography*, **12** (10), 1154–1158, doi:10.1175/1520-0485(1982)012<1154:OIMBCR>2.0.
788 CO;2.
- 789 Roach, C. J., D. Balwada, and K. Speer, 2018: Global observations of horizontal mixing from
790 argo float and surface drifter trajectories. *Journal of Geophysical Research: Oceans*, **123** (7),
791 4560–4575, doi:10.1029/2018JC013750.
- 792 Shchepetkin, A. F., and J. C. McWilliams, 2005: The regional oceanic modeling system (roms): a
793 split-explicit, free-surface, topography-following-coordinate oceanic model. *Ocean modelling*,
794 **9** (4), 347–404, doi:https://doi.org/10.1016/j.ocemod.2004.08.002”.
- 795 Smith, R. D., and P. R. Gent, 2004: Anisotropic Gent-McWilliams parameterization for ocean
796 models. *Journal of Physical Oceanography*, **34**, 2541–2564.

- 797 Solomon, H., 1971: On the Representation of Isentropic Mixing in Ocean Circulation Models.
798 *Journal of Physical Oceanography*, **1** (3), 233–234, doi:10.1175/1520-0485(1971)001<0233:
799 OTROIM>2.0.CO;2.
- 800 Starr, V. P., 1945: A Quasi-Lagrangian System of Hydrodynamical Equations. *Journal of Meteorology*,
801 **2** (4), 227–237, doi:10.1175/1520-0469(1945)002<0227:AQLSOH>2.0.CO;2.
- 802 Talley, L. D., and J.-Y. Yun, 2001: The role of cabbeling and double diffusion in setting the density
803 of the north Pacific intermediate water salinity minimum. *Journal of Physical Oceanography*,
804 **31** (6), 1538–1549, doi:10.1175/1520-0485(2001)031<1538:TROCAD>2.0.CO;2.
- 805 Treguier, A. M., I. M. Held, and V. D. Lariehev, 1997: On the parameterization of quasi-
806 geostrophic eddies in primitive equation ocean models. *Journal of Physical Oceanography*, **27**,
807 567–580.
- 808 Urakawa, L. S., and H. Hasumi, 2012: Eddy-resolving model estimate of the cabbeling effect on
809 the water mass transformation in the southern ocean. *Journal of Physical Oceanography*, **42** (8),
810 1288–1302, doi:10.1175/JPO-D-11-0173.1.
- 811 Veronis, G., 1975: *Numerical Models of Ocean Circulation.*, chap. The role of models in tracer
812 studies, 133–146. National Academy of Science.
- 813 Viktor Gouretski and K. P. Koltermann, 2004: Woce global hydrographic climatology. *Berichte
814 des BSH*, **35**, 1–52.
- 815 Walin, G., 1982: On the relation between sea-surface heat flow and thermal circulation in the
816 ocean. *Tellus*, **34** (2), 187–195, doi:10.1111/j.2153-3490.1982.tb01806.x.

- 817 Waterhouse, A. F., and Coauthors, 2014: Global Patterns of Diapycnal Mixing from Measurements
818 of the Turbulent Dissipation Rate. *Journal of Physical Oceanography*, **44** (7), 1854–1872, doi:
819 10.1175/JPO-D-13-0104.1, URL <http://dx.doi.org/10.1175/JPO-D-13-0104.1>.
- 820 Whitworth, T., and R. G. Peterson, 1985: Volume transport of the antarctic circumpolar current
821 from bottom pressure measurements. *Journal of Physical Oceanography*, **15** (6), 810–816, doi:
822 10.1175/1520-0485(1985)015<0810:VTOTAC>2.0.CO;2.
- 823 Witte, E., 1902: Zur theorie den stromkabbelungen. *Gaea: Natur und Leben*.

824 LIST OF FIGURES

825	Fig. 1.	Conceptual explanation of the two methods for computing neutral slopes and gradients. The red dots on the south and north casts represent the tracer points at which data is provided. The yellow stars are the T-grid data averaged on the vertical interface between the two casts. The purple square is where we wish to obtain values of the neutral slope and gradient. The black surface is an example of how a neutral surface could be oriented, which would lead to $N^2 \approx 0$, and problems for the local-method, which obtains its data from the data at the blue stars and blue circles. The non-local method obtains the approximate neutral surface as shown in green, and avoids the problems with a locally small N^2	42
833	Fig. 2.	A map (depth = 300 m) and transect (longitude = 215.5) of S_x (top) and S_y (below) for January. The dashed-blue line indicates the location of the transect (in the map) and the depth for which the map is plotted (in the transect). Positive slopes indicate neutral surfaces sloping upward to the north (for S_y) or east (for S_x). Black contours indicate Neutral Density γ^n contours.	43
838	Fig. 3.	A map (depth = 300m, top) and transect (longitude = 215.5, bottom) of the neutral Θ gradients in the x -direction $\nabla_N \Theta \cdot \hat{\mathbf{x}}$, for January. The transect is limited to 2 km depth, in order to show the more interesting parts. The dashed-blue line indicates the location of the transect (in the map) and the depth for which the map is plotted (in the transect). Positive Θ gradients increase from west to east. Black contours indicate Neutral Density γ^n contours.	44
843	Fig. 4.	As figure 3, but for $\nabla_N \Theta \cdot \hat{\mathbf{y}}$. When Θ gradients are positive, this indicates and increase of Θ when moving along the surface from along the surface south to north.	45
845	Fig. 5.	As figure 3, but for $\nabla_N \Theta \cdot \hat{\mathbf{z}}$. With positive Θ gradients increase from surface to bottom. When Θ gradients are positive, this indicates and increase of Θ when moving along the surface from the shallow to the deep part of the NTP.	46
848	Fig. 6.	The distribution of the values of the fictitious diffusivity $D^f(\text{m}^2 \text{s}^{-1})$ for the non-local method (blue), hybrid-method (orange), local-method (yellow) and σ_2 (purple). The thick vertical black line indicates values for $D^f = 10^{-5} \text{ m}^2 \text{s}^{-1}$. Black contours indicate Neutral Density γ^n contours.	47
852	Fig. 7.	A map (depth = 300m, top) and transect (longitude = 215.5, bottom) of $D^f(\text{m}^2 \text{s}^{-1})$ for the month January. The dashed-blue line indicates the location of the transect (in the map) and the depth for which the map is plotted (in the transect).	48
855	Fig. 8.	Water Mass Transformation due to Cabbeling (upper panel) and Thermobaricity (lower panel), using neutral gradients from for the non-local method (blue), hybrid-method (orange), local-method (yellow) and σ_2 (purple). Positive (negative) values indicate transformation into denser (lighter) water.	49
859	Fig. 9.	Eddy Heat transport $H(y)$ (A), $h(y, z = 1000)$ (B), $H(z)$ (C) using neutral gradients from for the non-local method (blue), hybrid-method (orange), local-method (yellow) and σ_2 (purple).	50
862	Fig. 10.	Description of a T-grid box.	51

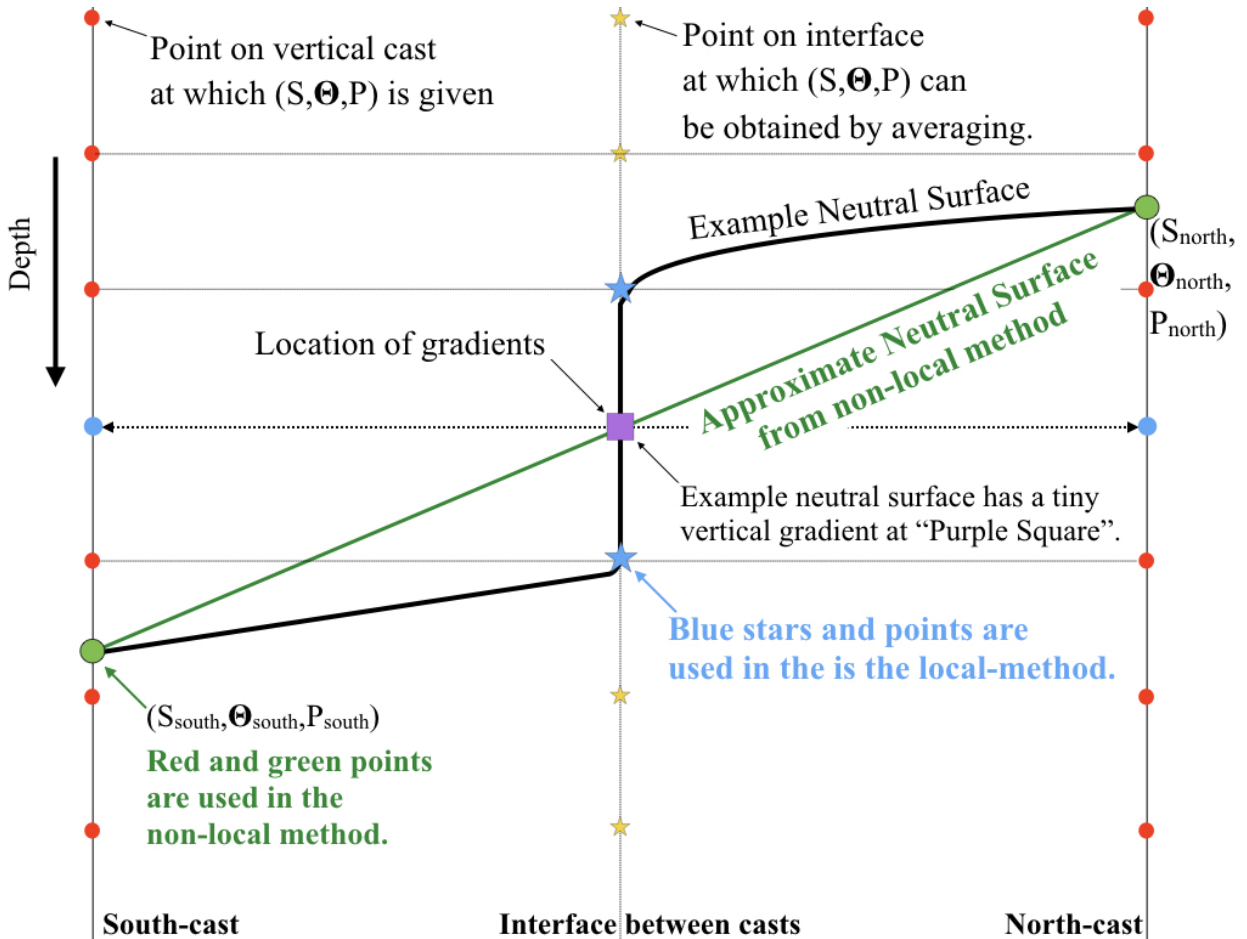
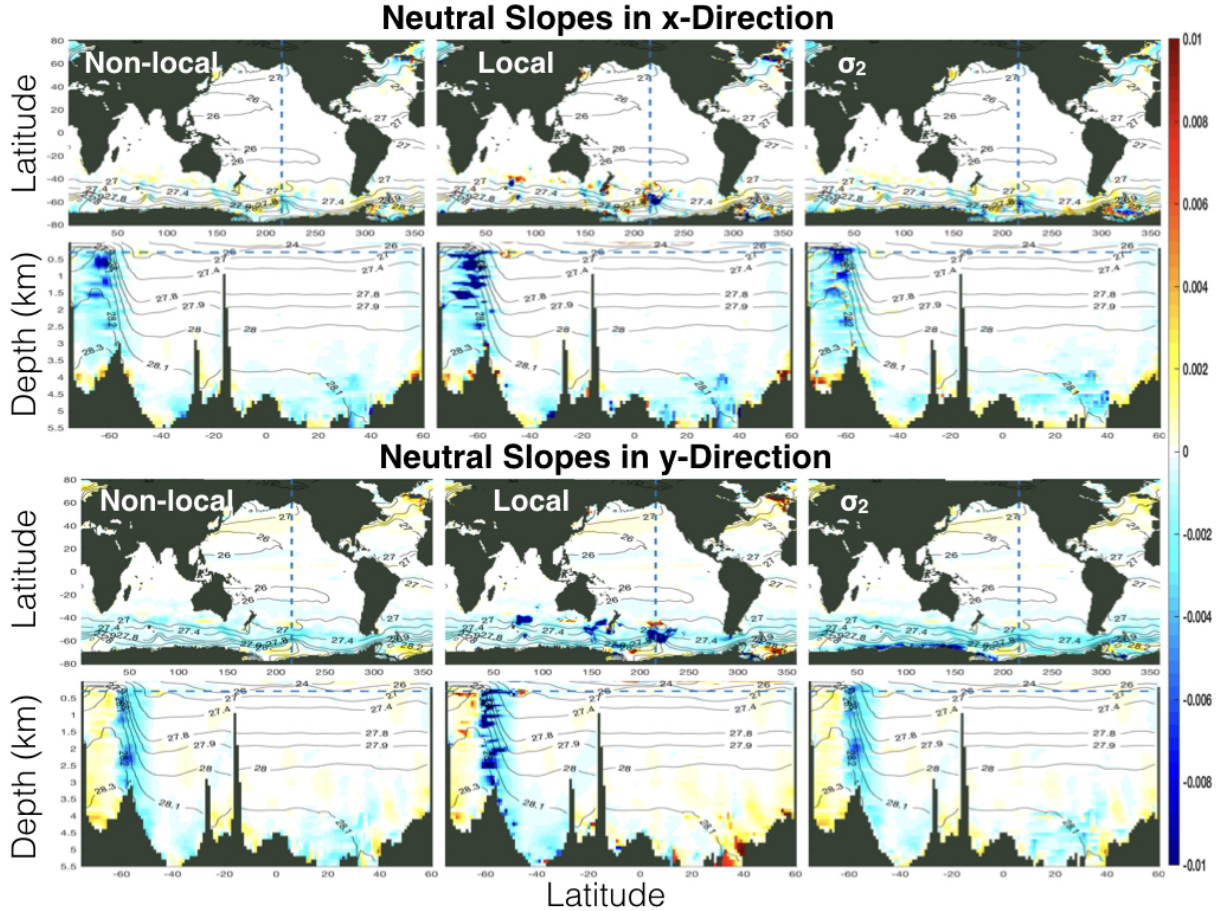
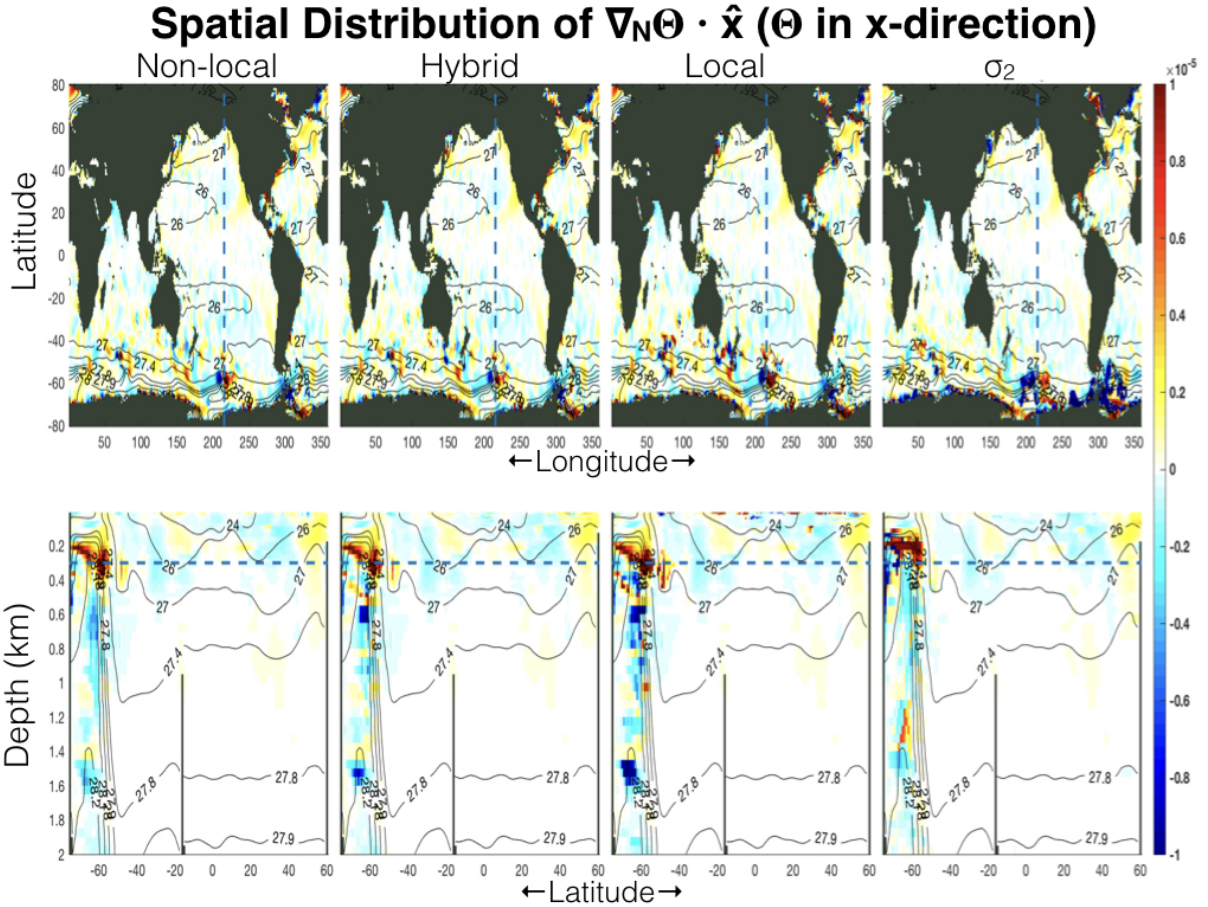


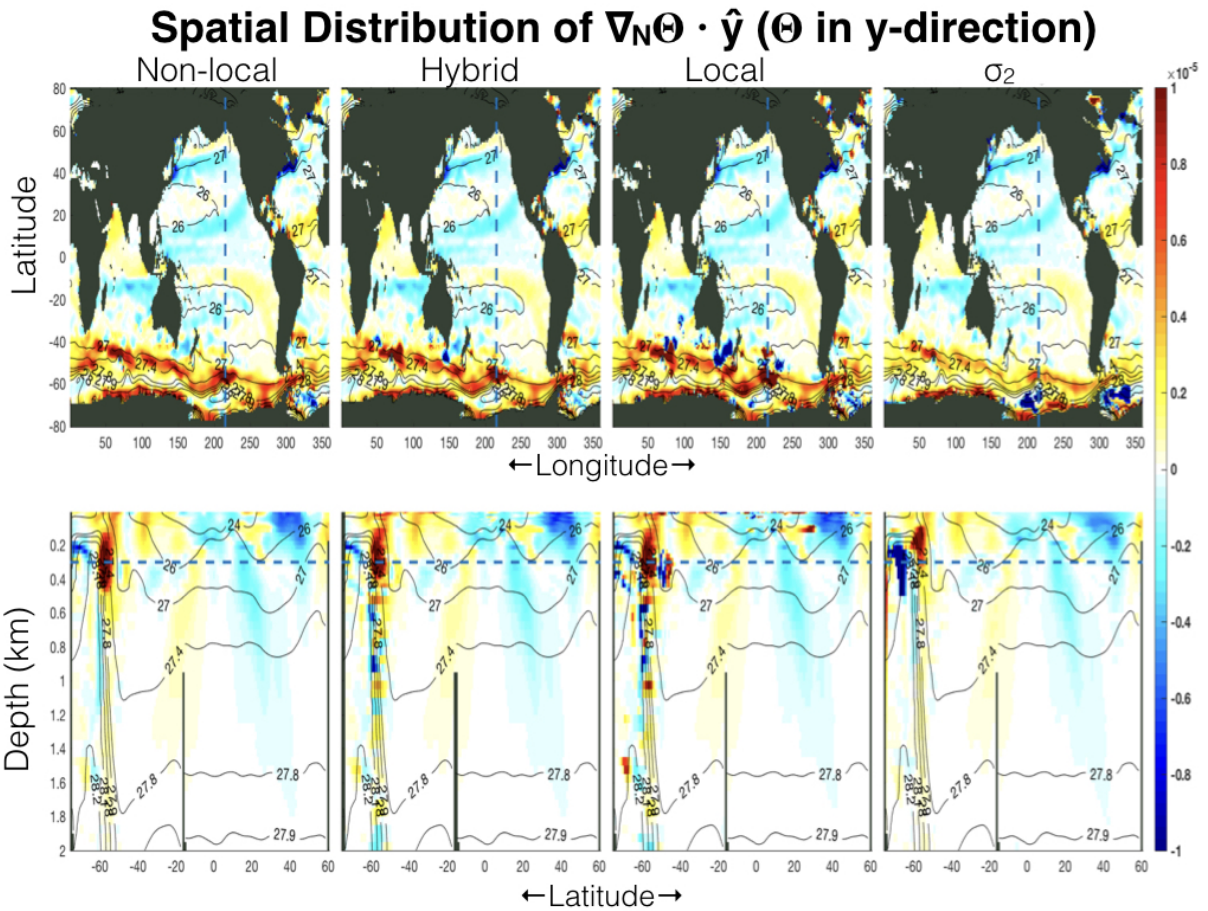
FIG. 1. Conceptual explanation of the two methods for computing neutral slopes and gradients. The red dots on the south and north casts represent the tracer points at which data is provided. The yellow stars are the T-grid data averaged on the vertical interface between the two casts. The purple square is where we wish to obtain values of the neutral slope and gradient. The black surface is an example of how a neutral surface could be oriented, which would lead to $N^2 \approx 0$, and problems for the local-method, which obtains its data from the data at the blue stars and blue circles. The non-local method obtains the approximate neutral surface as shown in green, and avoids the problems with a locally small N^2 .



870 FIG. 2. A map (depth = 300 m) and transect (longitude = 215.5) of S_x (top) and S_y (below) for January. The
 871 dashed-blue line indicates the location of the transect (in the map) and the depth for which the map is plotted (in
 872 the transect). Positive slopes indicate neutral surfaces sloping upward to the north (for S_y) or east (for S_x). Black
 873 contours indicate Neutral Density γ^n contours.



874 FIG. 3. A map (depth = 300m, top) and transect (longitude = 215.5, bottom) of the neutral Θ gradients in the
 875 x -direction $\nabla_N \Theta \cdot \hat{x}$, for January. The transect is limited to 2 km depth, in order to show the more interesting
 876 parts. The dashed-blue line indicates the location of the transect (in the map) and the depth for which the map
 877 is plotted (in the transect). Positive Θ gradients increase from west to east. Black contours indicate Neutral
 878 Density γ^n contours.



879 FIG. 4. As figure 3, but for $\nabla_N \Theta \cdot \hat{y}$. When Θ gradients are positive, this indicates an increase of Θ when
880 moving along the surface from along the surface south to north.

Spatial Distribution of $\nabla_N \Theta \cdot \hat{z}$ (Θ in z-direction)

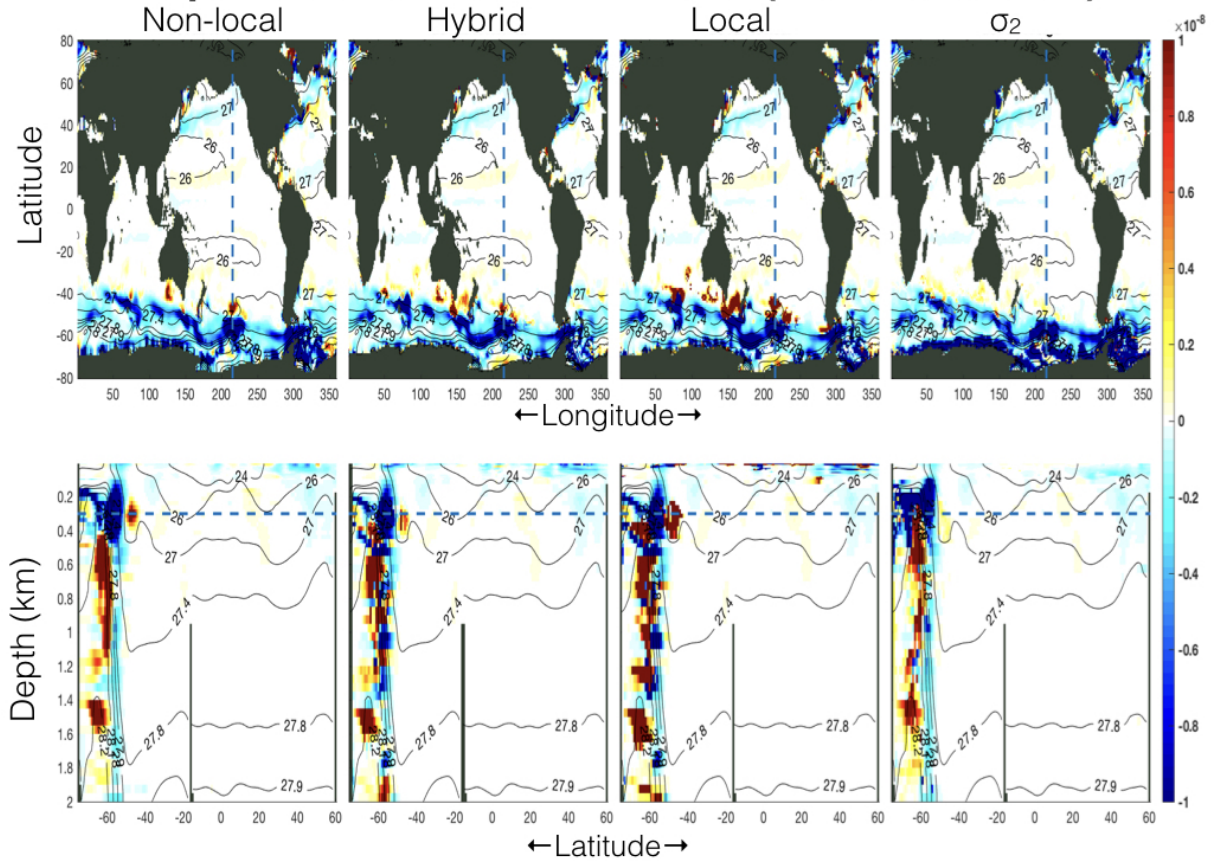


FIG. 5. As figure 3, but for $\nabla_N \Theta \cdot \hat{z}$. With positive Θ gradients increase from surface to bottom. When Θ gradients are positive, this indicates an increase of Θ when moving along the surface from the shallow to the deep part of the NTP.

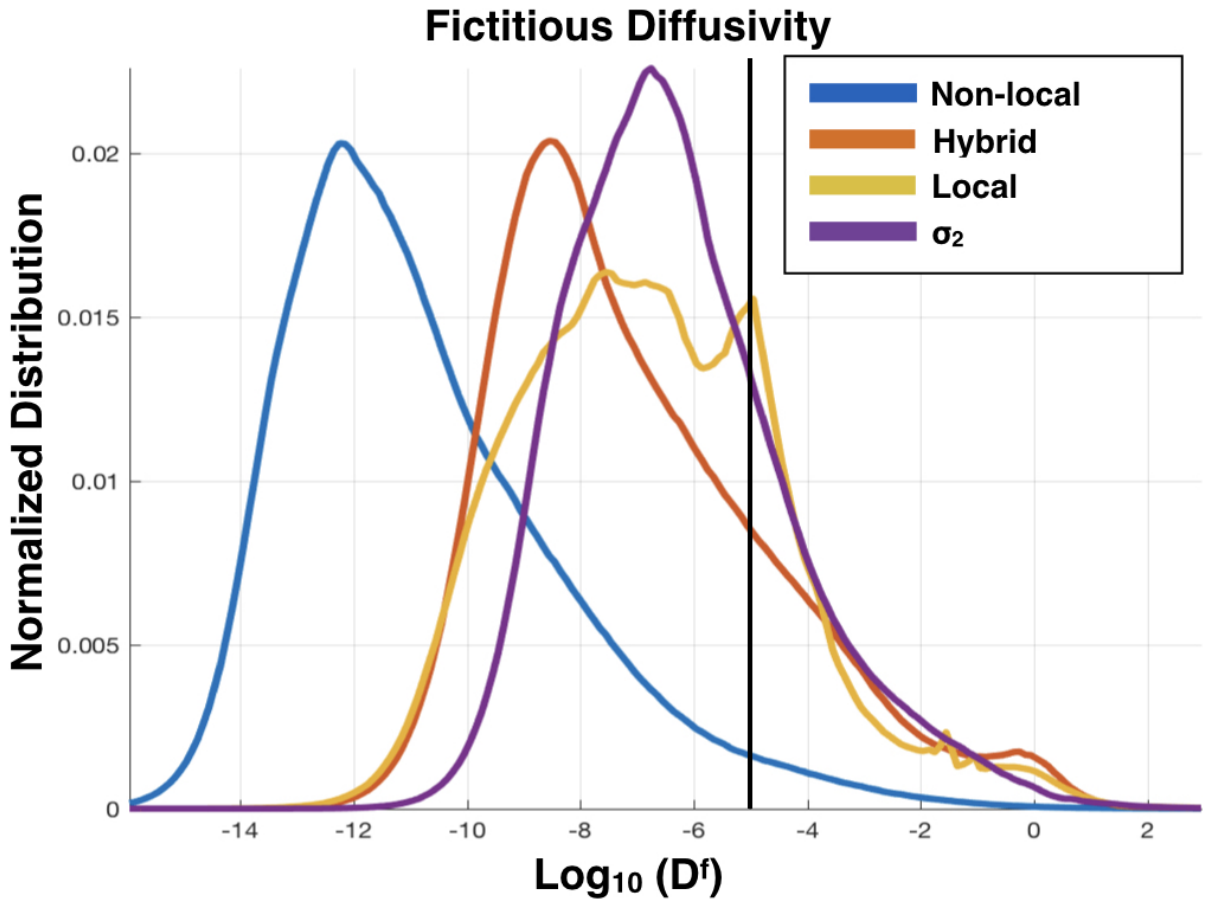


FIG. 6. The distribution of the values of the fictitious diffusivity D^f ($\text{m}^2 \text{ s}^{-1}$) for the non-local method (blue), hybrid-method (orange), local-method (yellow) and σ_2 (purple). The thick vertical black line indicates values for $D^f = 10^{-5} \text{ m}^2 \text{ s}^{-1}$. Black contours indicate Neutral Density γ^n contours.

Spatial Distribution of Fictitious Diffusivity

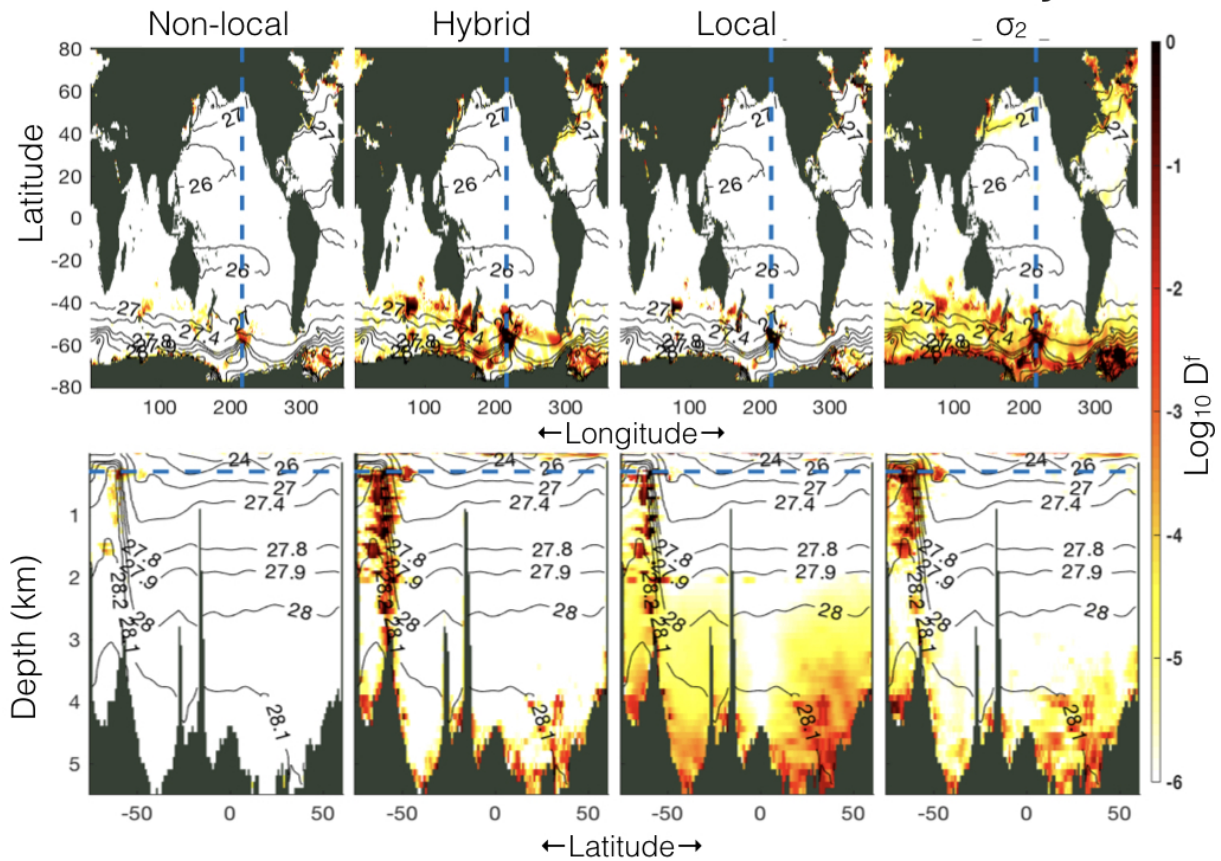


FIG. 7. A map (depth = 300m, top) and transect (longitude = 215.5, bottom) of $D^f(\text{m}^2 \text{s}^{-1})$ for the month January. The dashed-blue line indicates the location of the transect (in the map) and the depth for which the map is plotted (in the transect).

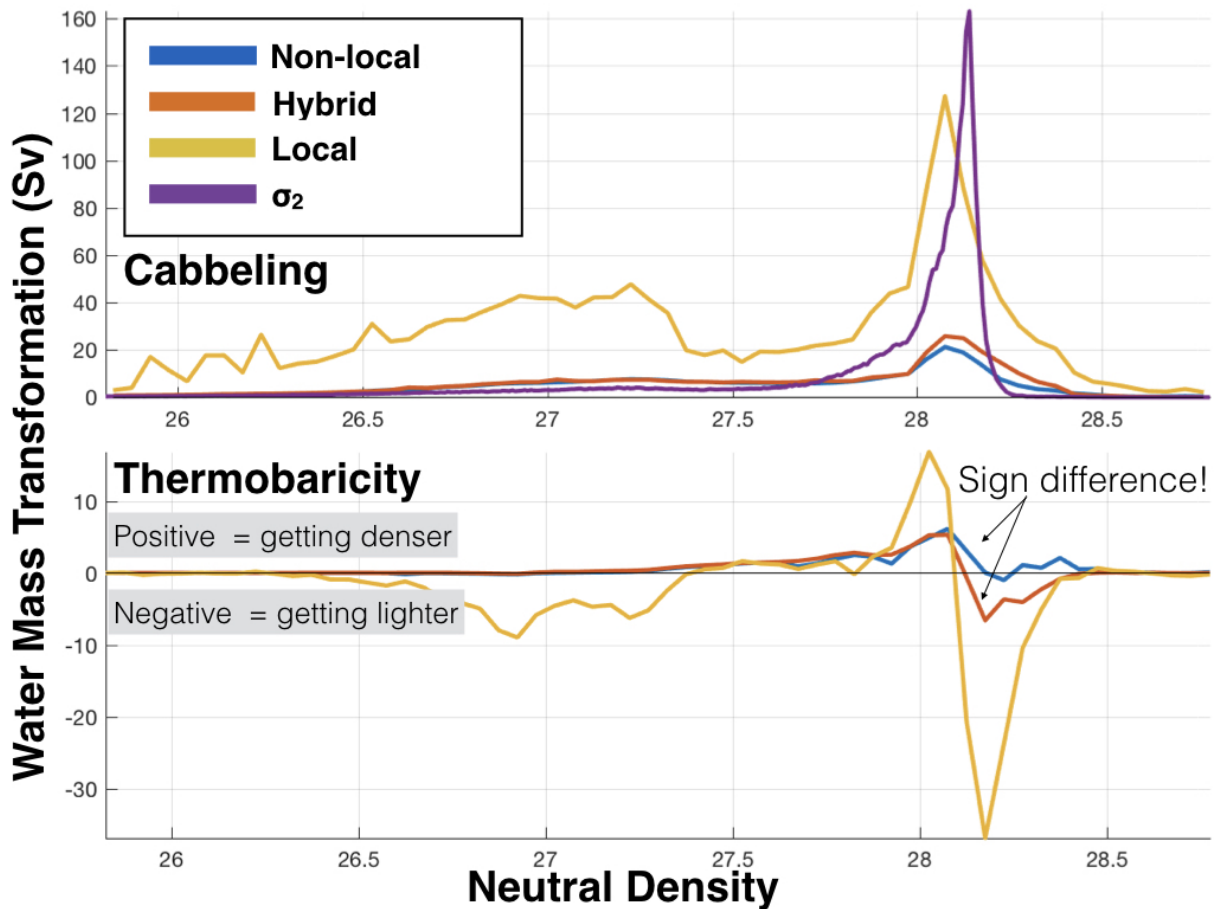


FIG. 8. Water Mass Transformation due to Cabbeling (upper panel) and Thermobaricity (lower panel), using neutral gradients from for the non-local method (blue), hybrid-method (orange), local-method (yellow) and σ_2 (purple). Positive (negative) values indicate transformation into denser (lighter) water.

Meridional and Vertical Heat Transports

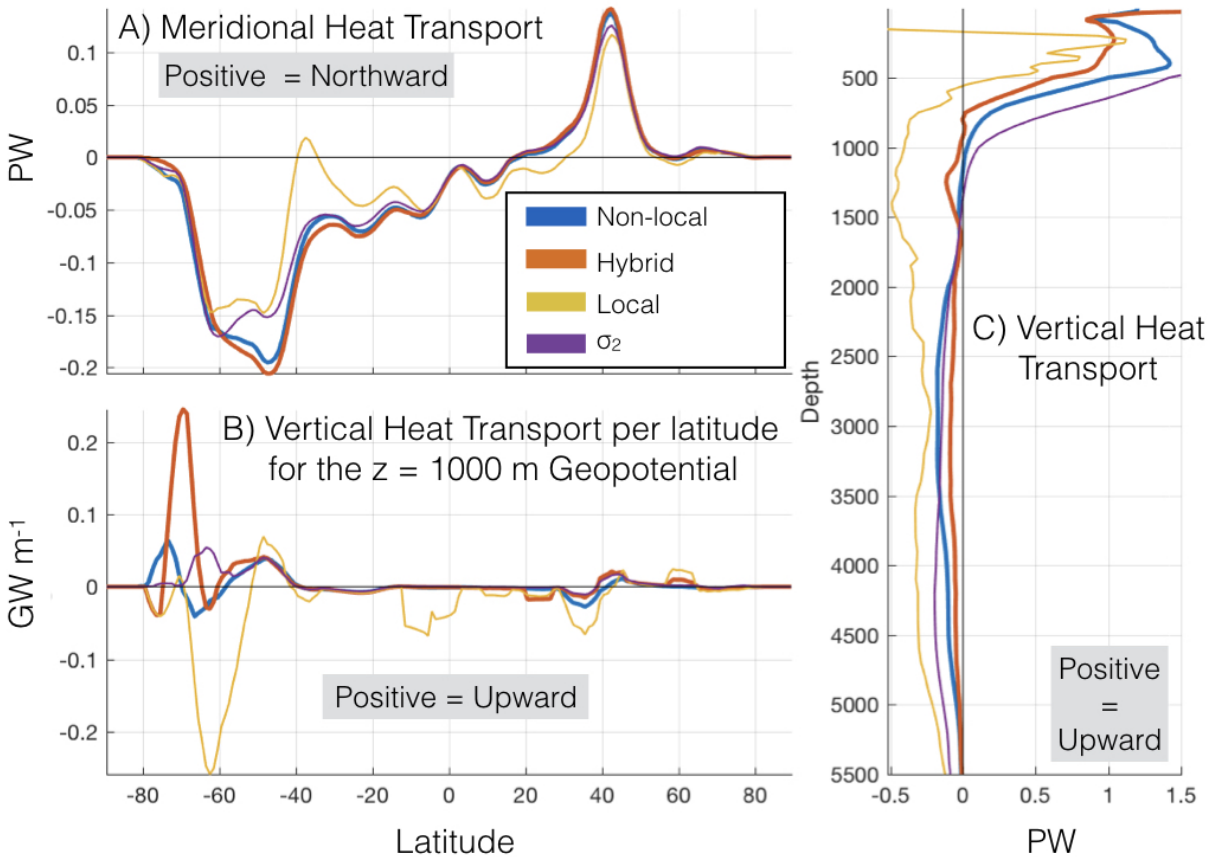


FIG. 9. Eddy Heat transport $H(y)$ (A), $h(y, z = 1000)$ (B), $H(z)$ (C) using neutral gradients from for the
 non-local method (blue), hybrid-method (orange), local-method (yellow) and σ_2 (purple).

Cartesian Coordinates. Finite volume representation for a T-grid

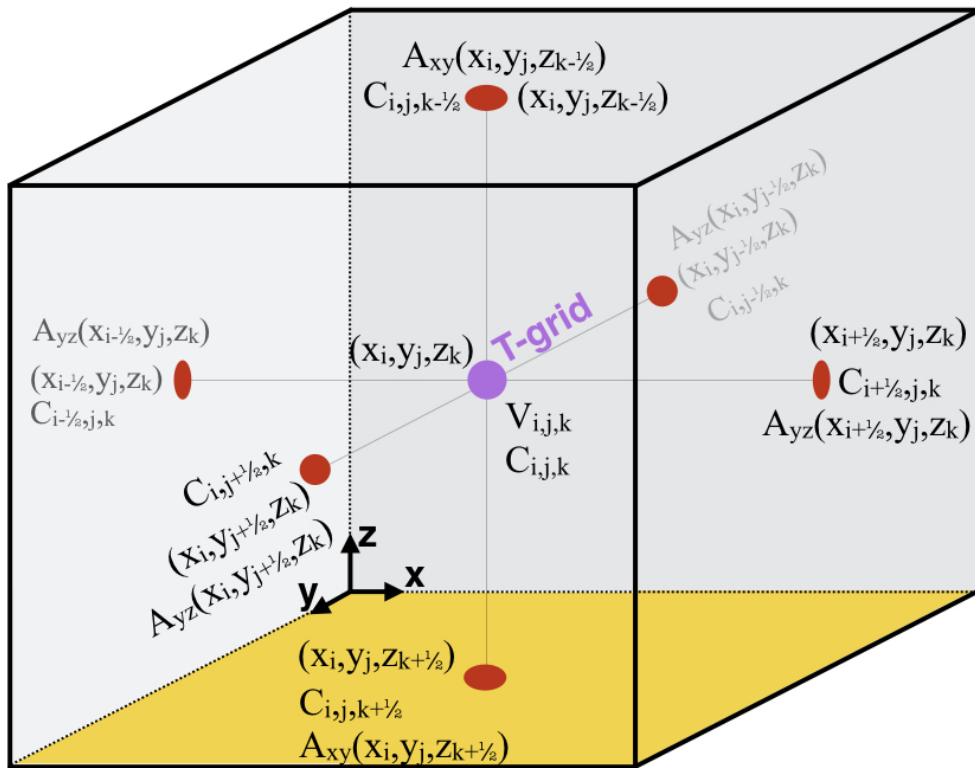


FIG. 10. Description of a T-grid box.